A Comparative Tradeoff of Electric Power System Architecture Reliabilities in CubeSat Satellites

by

Christopher A. Kudrick

Bachelor of Science, Electrical and Computer Engineering, University of Pittsburgh, 2006

Master of Science, Electrical Engineering, Gannon University, 2011

Submitted to the Graduate Faculty of the

Swanson School of Engineering in partial fulfillment

of the requirements for the degree of

Master of Science in Electrical and Computer Engineering

University of Pittsburgh

2021

UNIVERSITY OF PITTSBURGH

SWANSON SCHOOL OF ENGINEERING

This thesis was presented

by

Christopher A. Kudrick

It was defended on

October 22, 2021

and approved by

Dr. Brandon Grainger, Ph.D., Assistant Professor
Department of Electrical and Computer Engineering

Dr. Robert Kerestes, Ph.D., Assistant Professor
Department of Electrical and Computer Engineering

Dr. Alexis Kwasinkski, Ph.D., Associate Professor
Department of Electrical and Computer Engineering

Thesis Advisor: Dr. Brandon Grainger, Ph.D., Assistant Professor
Department of Electrical and Computer Engineering

A Comparative Tradeoff of Electric Power System Architecture Reliabilities in CubeSat Satellites

Christopher A. Kudrick, MS ECE

University of Pittsburgh, 2021

Small nanosatellites, such as CubeSats, represent an important population of satellites that are currently commissioned in various types of scientific research missions in space travel. CubeSats are small cubic satellites that can vary in size and are most commonly deployed in the "1U" size, measuring one cubic meter. CubeSats are important in scientific research as they follow a standardized design specification, known as the CDS, which aims to normalize the cost of development and deployment, as well as act as a baseline design specification for a community of researchers, students, and inventors.

The advent of CubeSat development has enabled thousands of researchers to conduct space missions, which had otherwise been too expensive and resource intensive. For CubeSats, the Electric Power System (EPS) has been documented as being the most unreliable sub-system in the CubeSat architecture. Further, it is the most critical sub-system, as a CubeSat cannot function without the EPS performing its intended functionality.

While the CDS provides guidelines for CubeSat development, there is flexibility. The intent of this thesis is to analyze the reliability impact of proposed alternative EPS architectures compared to the current implementation. Alternative architectures consist of the same components as the baseline, but are arranged in varying configurations and quantities. A comparative study is performed between ten alternative EPS architectures against a baseline by determining the failure rate and Mean Time To Failure (MTTF) for each configuration. Reliability calculations are

supported by determining each architecture minimal cut set and developing a corresponding Reliability Block Diagram. After, an analysis of the pros and cons between the alternative variants and the baseline is discussed. The proposed alternative architectures investigate the reliability impact of implementing distributed architectures, where redundant components and common connection busses are integrated to introduce varying levels of redundancy and operational flexibility.

Table of Contents

List of Tables

List of Figures

Acknowledgements

I'd like to begin these acknowledgements by recognizing the effort it took to get here. The past two years have been the most trying and difficult of my life. The majority of my study for this degree took place during the seemingly never-ending COVID-19 pandemic, in which I plan to defend this thesis directly during the two-year anniversary of this disaster (the pandemic still hasn't ended as of October 22, 2021). At nearly the beginning of this pandemic, my wife and I welcomed our first child into this world during the most uncertain time of our lives. Our anxieties and concerns were however no match against our excitement of welcoming a beautiful and healthy baby boy into the world. Many times, I never thought I'd be able to make it to this point but with my wife and son, I had such a positive influence and motivation to make it through.

That being said, I wouldn't have made it without the support of my professors, colleagues, and family. I'd like to thank Dr. Alexis Kwasinski, Dr. Robert Kerestes, Dr. Neal Clements, Dr. Paul Ohdonicki, Dr. Brandon Grainger, and John Paserba for their terrific courses that I enjoyed thoroughly throughout my study. Further, I'd like to thank my professional colleagues Dr. Adam Salih and Dr. Maxime Berger for their amazing support and mentorship throughout my years working at Bombardier Transportation. Also, I'd like to thank Dr. Brandon Grainger, my advisor throughout this process, for his support, leadership, and guidance.

Most importantly, I'd like to thank my wife Lauren for her support over the past 3 ½ years while I've studied at Pitt. Without her support and encouragement, I wouldn't be where I am and this goal would have not been a possibility.

This thesis, and the effort to get this point, is dedicated to my son, James. You inspire me to be the best person and father I can be. I hope you have the opportunity to read this one day and

it inspires you as much as you've inspired me. My dream for you is that you realize anything you set your sights on is achievable and that you make learning a lifelong endeavor. I love you and always will.

1.0 Introduction

While much smaller in scale and size, nanosatellites, such as the now common and widely commissioned “CubeSat”, face many of the same type of technical challenges in the design, implementation, and control of their electric power system as any larger power system might. A CubeSat is, as the name implies, a cubic shaped satellite that measures 10 cm per side and weighs approximately 1 kg [1]. This specific size and weight of CubeSat is given the nomenclature of a “1U” standard unit. CubeSats can be configured in multiples of the 1U unit, and are termed such as 2U, 3U, or 6U, which are multiples of the 1U baseline. Currently, launched CubeSats range in size of 0.25U to 27U and weigh approximately 0.2kg to 40kg. As of April 4, 2021, 1,553 CubeSats have been launched into space [2].

The first CubeSat design specification was proposed by aerospace engineer Jordi Puig-Sauri and Aeronautics and Astronautics professor Robert Twiggs in 1999, as an academic approach and tool to bringing the study and implementation of satellites to a more obtainable and practical level for university students. Since the advent of the CubeSat technology and implementation, space exploration has become more practical due to lower costs and a manageable size of satellites [3].

To be classified as a CubeSat and fit for space travel, designs must adhere to a set of standard design specifications, which is titled *CubeSat Design Specification,* referred to as CDS [4]. The CDS not only calls out system and subsystem design requirements, but testing and qualification requirements as well. The intent of these testing and qualification requirements are to ensure the safety of the Poly Picosatellite Orbital Deployer (P-POD), mission, and CubeSat itself. Having a standard design specification helps to normalize cost and has enabled a community

of inventors, professionals, students, and enthusiasts to share and leverage knowledge. Further, the standardization has enabled the use of Commercial off the Shelf (COTS) components to be implemented into designs. Using COTS components for design implementation is advantageous in maintaining reasonable cost figures in CubeSat development as well as lead time of components. However, this can limit some of the flexibility for design uniqueness.

A CubeSat shares the same type of power architecture as a typical microgrid might, albeit the system is in outer space. The CubeSat has distributed power generation using primarily Photovoltaic (PV) cells to charge a battery with a power electronics interface. A typical electric power system for a CubeSat consists of generation, storage, and control and distribution stages [5] which are designed to meet peak payload demands under both eclipse and non-eclipse of the sun operational phases. During sun phase non-eclipse periods, where the CubeSat is exposed to sunlight, the power generated by PV cells is split between payload instruments and a battery charging circuit. During eclipse periods, when the CubeSat is not exposed to sunlight, the stored energy in the battery is used to power the payload devices. For example, a typical CubeSat orbit around Earth takes roughly 100 minutes, where 62 minutes are during the sun phase [6]. Therefore, in this case, solar energy is both providing power for the CubeSat systems and payloads as well as charging the onboard power battery.

In satellite space missions, battery failures account for approximately 13% of the overall number of failures based on a study of the causes of power-related satellite failures [7]. Furthermore, in CubeSats, the second largest attributing failure during launch phase and the primary cause of failure during latter parts of the lifecycle is the Electric Power System, or EPS. The EPS, out of 7 categorized subsystems, attributes up to 44% of all documented failures in

CubeSats based on an extensive survey given to developers [8]. Batteries are a sub-component of the EPS.

The EPS consists of four primary components/subsystems, which will be referred to throughout this thesis as "Building Blocks":

- Fuel source for providing EPS power. In the case of a CubeSat, the fuel source is a PV array. Typically in a CubeSat, five PV panels are wired in series [11].
- DC-DC boost converter for managing power generated from the PV array. The DC-DC boost converter controller has a Maximum Powerpoint Tracking (MPPT) algorithm implemented in the microcontroller electronics to harvest maximum energy from the PV array. MPPT algorithms are well-adapted schemes for solar energy management and one such prescribed approach is described by A. Lashab et al [9].
- Battery for energy storage. In modern CubeSats and nanosatellites, the most common battery type is Lithium-Ion (Li-Ion) due to their superior energy and power density [10] than most other types.
- DC-DC converter to normalize voltage levels for various payloads and other subsystem components. These power supplies are typically a COTS switching or linear regulator [11] but does not necessarily need to be of these types.

There are various sub-components of the four subsystems listed above, such as a microprocessor, over-voltage protection devices, voltage and current sensing elements, and load switches, but these will be classified as supporting elements to the overall EPS within this thesis. The subsystems listed above will be considered as building blocks for investigation of various types of architectures against a baseline. **Figure 1** below displays a standard EPS block diagram

architecture of a CubeSat, and will be used as said baseline for comparison of all other architectures within this thesis.

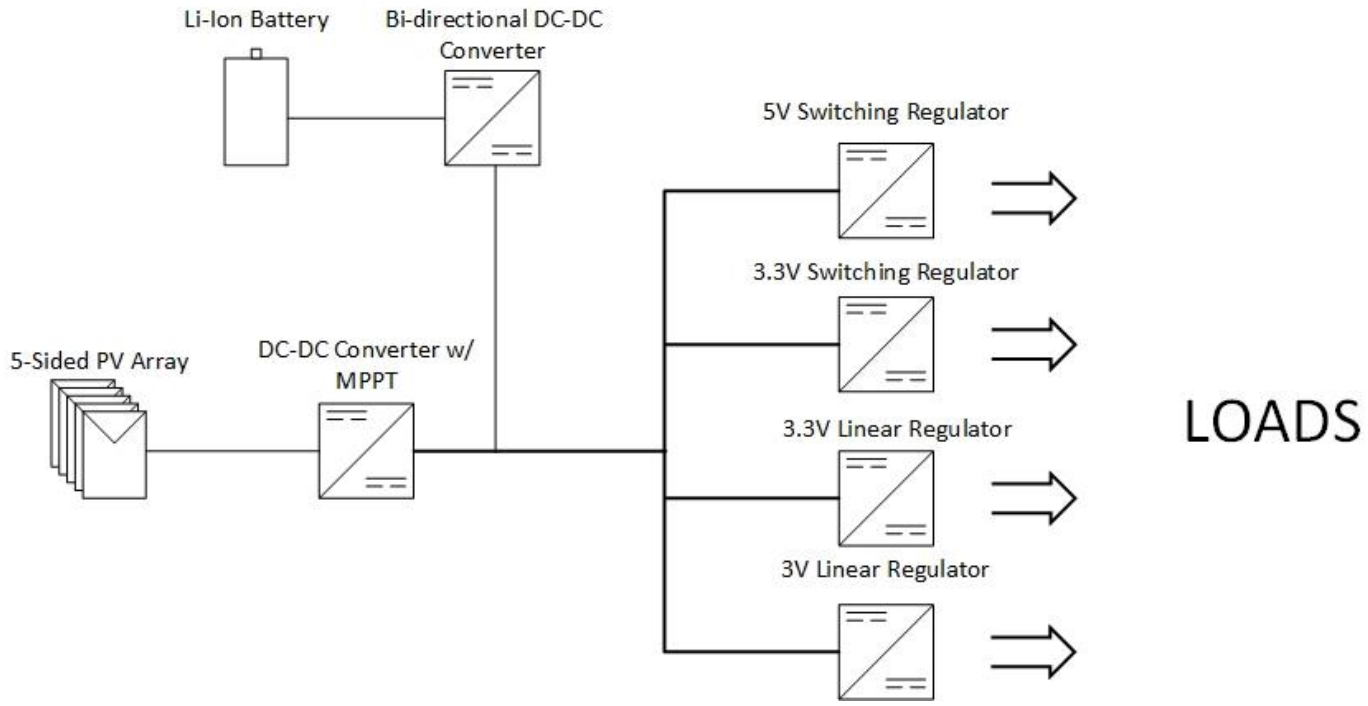

Figure 1—Traditional and baseline architecture block diagram for CubeSat EPS

With the traditional architecture displayed in **Figure 1**, there are several single points of failure; that is, if one of these components is to fail during any phase of a CubeSat launch or mission, the EPS would no longer perform its intended function, and the CubeSat mission would fail. However, if alternative architectures that meet the requirements set forth in the CDS were proposed, they can be compared against the standard architecture baseline and ranked according to their reliability. Said study could be used to develop and realize a new architecture, derivative of the baseline in **Figure 1**, to improve upon the failure rates of the EPS for CubeSats stated earlier in this section.

There are several important reasons as to why an improvement in CubeSat EPS reliability is advantageous. First and foremost, even a small improvement can mean the difference between

a successful or failed mission. The EPS is vital to the overall system operation, and loss of function can mean an entire satellite system failure. This is opposed to loss of payload, which may not be vital for the functionality of other payloads or subsystems. In other words, if a non-vital payload fails, the CubeSat may maintain functionality but at reduced performance or with the loss of specific experimental data collection, for example.

Another driving factor for improving CubeSat EPS reliability is in seizing the opportunity for exploring new frontiers of space. The large majority of CubeSat deployment is in Low Earth Orbit (LEO), which is considered anywhere in the range of 90 – 600 miles above the surface of the Earth. However, there are many different functions a CubeSat could serve for exploring outside of Earth orbit, such as Mars. Some functions a CubeSat orbiting Mars could provide includes weather monitoring, atmospheric profiling, gravity field data collection, and lightning detection [12], to name only a few. Deployment of CubeSats to Mars can take several months if not more than a year, considering the amount of time it takes for a deployment Mother Ship to reach Mars orbit. Guaranteeing an acceptable reliability for such a mission is critical for the viability of CubeSat use in exploring further reaches of space beyond Earth.

In this thesis, ten EPS architectures will be proposed as potential alternatives for the baseline. Each of these alternative architectures will have the same capability as the baseline, but they will either be arranged in a different manner, additional components will be added, or a combination of both. These reconfigurations or additions to the baseline will aim to improve the reliability of the CubeSat EPS architecture. It will be investigated if each alternate architecture does in fact improve the reliability relative to the baseline and with what potential tradeoffs that may exist. It is not the purpose of this thesis to investigate control and electrical integration of each architecture, but to determine whether or not it may be beneficial to take the next steps for

further research and development of the alternative. It is also not the purpose of this thesis to evaluate what causes individual component or subsystem failures, and therefore it is considered that all alternative EPS architectures are subjected to the same exact operating conditions as the baseline. The results of the analysis will all be ranked relative to the baseline according to their reliability figure.

For each architecture, an overall reliability figure will be established based on the subsystems and their arrangement within the EPS. The final reliability figure for each proposed architecture will be ranked against one another. A discussion regarding suitability of the best ranking architectures will discuss positive and negative tradeoffs against the baseline architecture. The overall purpose of this thesis is to provide a relative comparison of alternate EPS architectures against a baseline based on how well their reliability ranks.

Chapter 2.0 will introduce the logic, mathematics, and tools used to develop a reliability figure for the EPS architectures. The approach for determining points of failure as well as the introduction of the concept and use of a Reliability Block Diagram (RBD) will be explored. For each EPS architecture, minimal cut sets will be determined to aid in the RBD development. The breakdown for developing reliability figures for the EPS architecture building blocks will be outlined. The reliability figures for building blocks will be expressed in Mean Time to Failure (MTTF) and will feed the RBD for an overall EPS reliability. The overall architecture under consideration will have a reliability figure presented in MTTF.

Chapter 3.0 will present the ten alternative EPS architectures for evaluation. Each EPS architecture will be represented by a System Block Diagram (SBD) with a description of the configuration and how it differs from the baseline. A matrix categorizing the amount of building block components and their configurations per EPS architecture will be presented. The matrix will

allow for easy comparison between all configurations and will act as a reference throughout the remainder of the thesis.

Chapter 4.0 will present the comparative reliability analysis using the methodology and equations outlined in previous chapters. A concept called *minimal cut set* will be presented for each architecture as well as the corresponding RBD. The minimal cut sets will be used to develop the RBD for each EPS. And with the RBD, the governing equations for MTTF and failure rate will be developed. A matrix will be presented displaying the resulting reliability figures for each EPS architecture.

Chapter 5.0 will summarize and present conclusions from the study. A comparison will be presented for the alternative architectures to the baseline. A recommendation based on improved reliability figures, assumed cost comparison to the baseline, and sound engineering judgment will be presented.

2.0 Logic, Mathematics, and Tools for Analysis

2.1 Reliability Block Diagram

To determine the MTTF reliability figure for each EPS architecture, several tools and methods will be employed. As mentioned in the introduction, the baseline EPS architecture has single points of failure; that is, components that if failed, the entire system will be considered failed, as the system can no longer achieve its intended function. Consider **Figure 2**, which highlights an example of a single point of failure for the baseline EPS from **Figure 1** when the DC-DC converter fails.

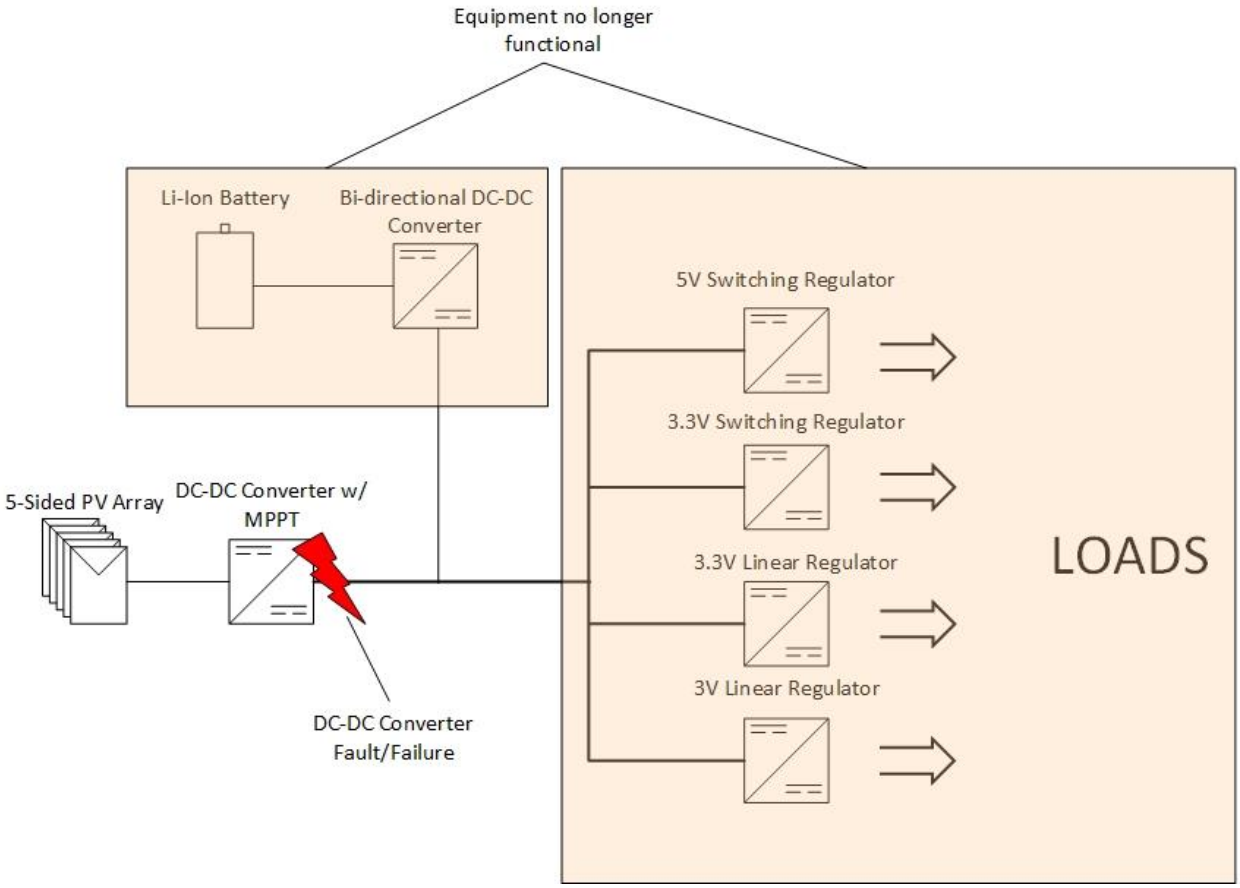

Figure 2—Baseline architecture displaying single point of failure with battery failure

To improve reliability, it is a goal to eliminate the single points of failure within the system, with the idea that more than one component must fail for the system to fail (or, a higher reliability component can be used in its place, but it is not the intent of this thesis to investigate alternatives from the defined Building Blocks). In general, re-configuring an architecture as such is likely to improve the reliability of the system, as long as the single point of failure is replaced by components, when combined in their functionality, have a better overall reliability. There are specific methods for calculating the system reliability which will be outlined.

One method for quantifying the reliability of a system is to use a Reliability Block Diagram. An RBD is a pictorial way of illustrating the functional state of a system using functional blocks

with an input and output. In an RBD, the state of each functional block is either *failed* or *functioning*. In the case of this thesis, the defined building blocks can be considered as the functional blocks in the RBD. If the building block is functioning, it is stated that *you can pass through the functional block* [13]. For example, if the Li-Ion battery in the EPS was functioning such that it was both accepting and providing charge under the desired loading conditions, it is stated that you can pass through the battery in the RBD. For the entire system, if you cannot pass through from the start to finish in the RBD from left to right, the system is not functioning and in other words has failed. If you can pass through from start to finish, the system is stated to be functioning. An RBD is similar in concept for passing from left to right as a logic diagram. The mathematics used in the construction of the RBD and throughout this analysis are detailed in the following sections.

2.2 State Variables, State Vectors, and Structure Functions

It is important to note the distinction between a system block diagram, such as in **Figure 1**, versus an RBD. An RBD illustrates a logical diagram of the components in a system merely to outline the functional state of the system. For a system of *n* distinct elements, such that for $i = 1, 2, 3, \ldots, n$, the state of each element in the RBD is represented by what is called a *state variable*, x_i:

$$x_i = \begin{cases} 1 \text{ if item } i \text{ is functioning} \\ 0 \text{ otherwise} \end{cases} \quad \textbf{(2-1)}$$

The makeup of all elements in the system, $x = (x_1, x_2, x_3, \ldots, x_n)$ is called the *state vector*. The overall state of the system, whether it is functional or non-functional, is described by what is termed the *structure function*, $\phi(x)$, which is a function of the state vector:

$$\phi(x) = \begin{cases} 1 \text{ if the system is functioning} \\ 0 \text{ otherwise} \end{cases} \quad \textbf{(2-2)}$$

For complex systems, such as the EPS architecture for the CubeSat, breaking the RBD down into the structure function is the first step to determining the overall system reliability.

Elements in an RBD are arranged in two manners: either in parallel or in series. Complex combinations of both will ultimately make up the desired RBD for a system. For example, sets of elements may be grouped such that three elements are in parallel and that grouping is in series with more sets of elements in parallel.

For a series-arranged group of elements, this grouping is said to be functioning only if all of its elements are functioning. The structure function representing this functionality is described as

$$\phi(x) = x_1 \cdot x_2 \cdots x_n = \prod_{i=1}^{n} x_i \quad \textbf{(2-3)}$$

where *n* is the total number of elements in the series arrangement. The structure function $\phi(x) = 1$, which represents a functioning system, when all elements of $x_n = 1$ in this relationship. Conversely, if any element of $x_n = 0$, the structure function $\phi(x) = 0$. **Figure 3** represents an example of an RBD with all elements in series.

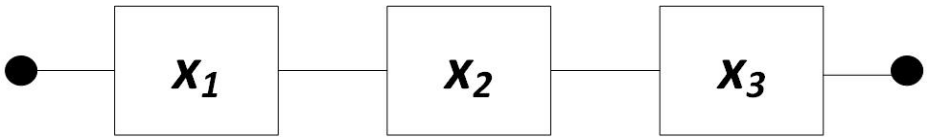

Figure 3—RBD with all elements in series

For a parallel-arranged group of elements, this grouping is said to be functioning if any one of in the grouping is functioning. The structure function representing this functionality is described as

$$\phi(x) = 1 - (1 - x_1)(1 - x_2) \cdots (1 - x_n) = 1 - \prod_{i=1}^{n}(1 - x_i) \quad \textbf{(2-4)}$$

where *n* is the total number of elements in the parallel arrangement. The structure function $\phi(x)$ = 1, which represents a functioning system, when any element of x_n = 1. Conversely, if all elements x_n = 0, then the structure function $\phi(x)$ = 0. **Figure 4** represents an example of an RBD with all elements in parallel.

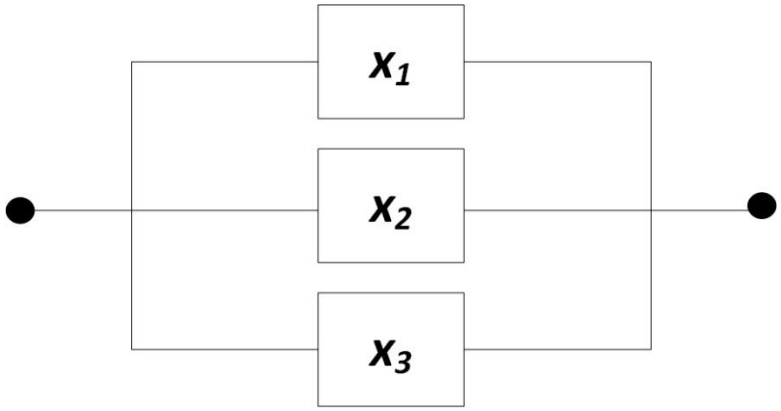

Figure 4—RBD with all elements in parallel

Using a combination of series and parallel systems in an RBD to create an overall structure function, a quantification of a system reliability can begin to be made. As an example, **Figure 5** displays an RBD with a combination of series and parallel elements, which will be a typical configuration for the various EPS architectures under consideration.

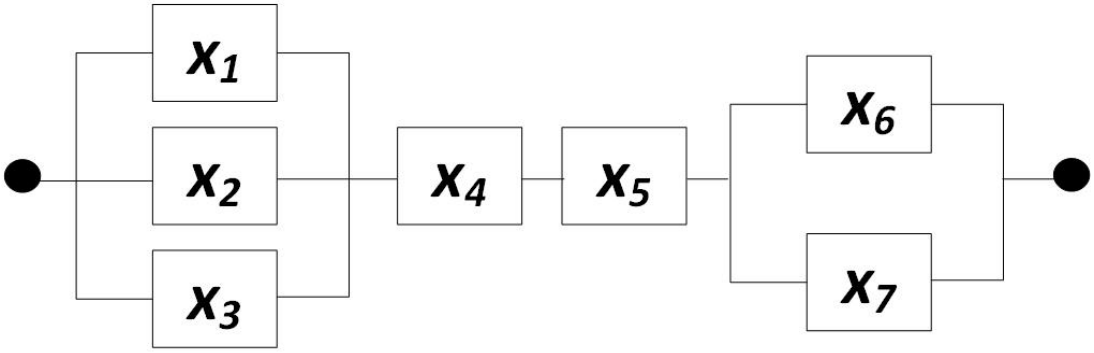

Figure 5—RBD with series and parallel element combinations

The concept for the system reliability, termed *survivor function*, *R(t)*, exists for a system that is nonrepairable. In the case of a CubeSat EPS, the system is in fact nonrepairable; as once it fails, the mission is failed and the device will not be returned home. The survivor function can be derived in part by the structure function and is used to further quantify the system reliability. The survivor function and Mean Time to Failure (MTTF), will be explored more in the next section.

2.3 Quantifying the System Survivor Function, Reliability and Mean Time to Failure

For this thesis, it is assumed that the state variables x_i described in the previous section are both random and depend on time, *t*. Therefore, each state variable will be referred to and written as $X_i(t)$, depicting them as a function of time. The series of all state variables x_i, referred to earlier as the state vector, will subsequently be written as $\boldsymbol{X}(t)$, indicating a vector of elements that vary in time. The reliability of item *i* at time *t* is denoted as $p_i(t)$, and is equal to the mean value of $X_i(t)$ [13]. From [13], it is stated that the system reliability, $p_S(t)$, is the mean value of the structure function of the time-varying state variables $X_i(t)$. Therefore, the system reliability of a series system, based on the mean value of the structure function, is defined as

$$p_{S,s}(t) = E\big[\phi\big(\boldsymbol{X}(t)\big)\big] = \prod_{i=1}^{n} E\big[\phi\big(X_i(t)\big)\big] = \prod_{i=1}^{n} p_i(t) \qquad \textbf{(2-5)}$$

And likewise, for a parallel system, is defined as

$$p_{S,p}(t) = E\big[\phi\big(\boldsymbol{X}(t)\big)\big] = E\left[1 - \prod_{i=1}^{n}\big(1 - X_i(t)\big)\right] = 1 - \prod_{i=1}^{n}\big(1 - p_i(t)\big) \qquad \textbf{(2-6)}$$

Since it is established that the CubeSat EPS system is nonrepairable, the item reliability $p_i(t)$ is equal to what is known as the *survivor function, $R_i(t)$,* and is exponentially distributed [13] with a constant failure rate λ_i:

$$p_i(t) = R_i(t) = e^{-\lambda_i t} \tag{2-7}$$

Two possible ways to quantify the overall reliability of a system are by the actual reliability, which is the probability that the system will operate as intended, or the Mean Time to Failure (MTTF), which is the average time a system can be expected to operate before a failure occurs. In both cases, the attributes of all elements in the system make up these figures. The reliability function for a system, $R_S(t)$, is calculated in the same exact way for series and parallel systems as the structure function is. The reliability for a series system is given as

$$R_{S,s}(t) = \prod_{i=1}^{n} R_i(t) = \prod_{i=1}^{n} e^{-\lambda_i t} = e^{-((\sum_{i=1}^{n} \lambda_i)t)} \tag{2-8}$$

and for a parallel system is given as

$$R_{S,p}(t) = 1 - \prod_{i=1}^{n} \big(1 - R_i(t)\big) = 1 - \prod_{i=1}^{n} \big(1 - e^{-\lambda_i t}\big) \tag{2-9}$$

In both cases, $R_S(t)$ is called the *survivor function.* As it is seen from (2-8) for a series system only, the overall system failure rate can be easily calculated by adding each constant failure rate:

$$\lambda_{Series} = \sum_{i=1}^{n} \lambda_i \tag{2-10}$$

Using the relationships given for the survivor function and provided in [13], the MTTF is calculated by

$$MTTF = \int_{t=0}^{\infty} R_S(t)dt \tag{2-11}$$

For a series system, calculating the MTTF as per (2-11) is straight forward

$$MTTF_{Series} = \frac{1}{\lambda_S} = \frac{1}{\sum_{i=1}^{n} \lambda_i} \quad \textbf{(2-12)}$$

However, (2-12) is not valid for a parallel system. In a parallel system, even if all items used have constant failure rates, the overall system does not have a constant failure rate [13]. For just two items parallel in a system, calculating the MTTF as per (2-11) becomes

$$MTTF_{Parallel} = \frac{1}{\lambda_1} + \frac{1}{\lambda_2} - \frac{1}{\lambda_1 + \lambda_2} \quad \textbf{(2-13)}$$

and the survivor function of two items in parallel, $R_{S,p}(t)$, can be given by

$$R_S(t) = e^{-\lambda_1 t} + e^{-\lambda_2 t} - e^{-(\lambda_1+\lambda_2)t} \quad \textbf{(2-14)}$$

This relationship for both MTTF and the survivor function as well as the similar equations for series systems will be used directly for quantifying the proposed EPS architectures in *Chapter 3*.

The relationship for determining the MTTF for parallel systems with more than two items becomes slightly more complex, but the concept and relationships of a *koon* structure ("k" out of "n") will be used.

2.4 *koon* Identical Structures

An effective and straightforward way to analytically quantify the survivor function and MTTF for parallel systems is by the relationship for *koon* structures. *koon* stands for "k" out of "n", which means that for a parallel structure with identical components, *k* out of the *n* total components must be functioning for the overall structure to function. If more than *k* elements have failed, the system or structure is considered to be not functional. In this thesis, the architectures to be proposed in *Chapter 3.0* will not have more than two non-identical components. In these

situations, the relationship given in (2-13) and (2-14) cannot be used to determine the MTTF and survivor function, respectively. Therefore, the *koon* relationship can be leveraged to first determine the survivor function of this structure, which can then easily be broken down into the MTTF. The survivor function for a *koon* parallel system with more than two items, of which these items are all identical, is given in [14] by

$$R_{S,p}(t) = \sum_{j=k}^{n} \binom{n}{j} e^{-j\lambda_i t}\left(1 - e^{-\lambda_i t}\right)^{n-j} \quad \textbf{(2-15)}$$

In (2-15), n is the total amount of elements in the parallel structure and j is the total number of elements that must be functioning in this parallel structure for the system to be considered fully operational. For this thesis, a *koon* structure will need to only have 1 out of n elements functioning properly for the system to operate as intended. With that in mind, (2-15) now becomes

$$R_{S,p}(t) = \sum_{j=1}^{n} \binom{n}{1} e^{-\lambda_i t}\left(1 - e^{-\lambda_i t}\right)^{n-1} \quad \textbf{(2-16)}$$

for the case of this thesis when there are more than two identical elements in a parallel structure. Substituting (2-16) into the equation for MTTF, (2-11), and performing mathematical substitution as outlined in [21] yields the following

$$MTTF_{k/n} = \sum_{j=k}^{n} \binom{n}{j} \int_0^{\infty} e^{-\lambda_i t j}\left(1 - e^{-\lambda_i t}\right)^{n-j} dt = \frac{1}{\lambda}\sum_{j=k}^{n} \frac{1}{j} \quad \textbf{(2-17)}$$

which can easily be used to determine the MTTF for a *koon* parallel system with 1 out of n elements required for functionality. This in turn can be used to determine the failure rate, λ_p, of this reduced parallel system. Throughout this thesis, a combination of (2-13), (2-14), (2-16), and (2-17) will be used to quantify the survivor function, MTTF, and failure rate of parallel structures within the associated RBD for the various EPS architectures under consideration. The goal of working with the RBD will be to reduce parallel structures to a single series element and then adding the failure

rate and MTTF of that element to other series elements in the RBD as per equations (2-10) and (2-12), respectively. By doing so, reliability metrics can be determined to quantify the viability of each EPS architecture under consideration.

To aid in developing these types of relationships for both parallel and series structures for a system represented in an RBD, the EPS architecture minimal cut sets will be determined.

2.5 Minimal Cut Sets

A *cut set* is defined as "a set of basic events whose (simultaneous) occurrence ensures that the top (or intended) event occurs" [13]. In other words, if all of the items in a structure function, which can represent a cut set, are operating as intended, the overall system will function as intended. Separating out into cut sets is a good way to develop an RBD for a system by breaking it down in a systemic and structured way. For this thesis, determining what is called a *minimal cut set* or *sets* for each EPS will aid in determining the overall RBD for that specific architecture. A cut set "is said to be minimal if the set cannot be reduced without losing its status as a cut set" [13]. In other words, a minimal cut set is the minimum number of components in a structure function that must be operational for the overall system to be considered functioning as intended. If one element in the minimal cut set fails, then that specific cut set has failed.

To aid in development of the RBD for each EPS, minimal cut sets, of which there will be multiple for each architecture, will be determined. Minimal cut sets for each architecture will be summarized in a corresponding table. The RBD of each architecture can then easily be tied back to the table of minimal cut sets for reference. Each minimal cut will be represented in the corresponding RBD as parallel elements (if there is more than one element in the cut set) or a

single element (if there is only one element in the cut set). All of the cut sets will then be combined in series. Ultimately, a structure function and RBD can be developed as a combination of series and parallel elements or structures. The governing relations defined earlier in this chapter will be used to develop the survivor function for each EPS architecture under consideration.

2.6 Determining Reliability Metrics for EPS Building Blocks

In practice, determining such parameters as the survivor function or MTTF for a component or a system largely depends on two methods for data collection: either through experiment and reliability testing or gathering information from published data. The former is not the scope of this thesis. The latter method will be employed using various methods, which will be outlined per building block. Components such as wiring harnesses, power connectors, cable terminals, control electronics, and other smaller components required to build the CubeSat EPS architecture will not be compared in the reliability study; only the major building blocks outlined earlier will be used in comparison.

2.6.1 DC-DC Boost and DC-DC Converter

The DC-DC Boost and DC-DC Converter building blocks will be considered as being made up of the same components. A *Buck-Boost* power converter will be considered as employed for both the DC-DC Boost Converter and DC-DC converter building blocks. A buck-boost converter can perform either functionality depending on how it is controlled. Furthermore, in consideration

of the traditional/baseline architecture, a buck-boost converter will be used to represent the 5V Switching Regulator, 3.3V Switching Regulator, 3.3V Linear Regulator, and 3V Linear Regulator.

A buck-boost converter is capable of "bucking" (reducing) or "boosting" (increasing) an input voltage level. The function of the buck-boost converter in all cases of the CubeSat EPS will be to regulate the voltage of a building block to a desired level. This is critical in all areas of the EPS. For example, the buck-boost converter will be used to boost the voltage supplied from the PV array and will be considered to have an MPPT algorithm implemented in its controller. Further, it is assumed that for this study the buck-boost converter will have the right load balancing control capabilities and can regulate the output voltage for increased load scenarios for EPS architectures that implement converter redundancy as a means to improve reliability.

To determine the DC-DC Boost, DC-DC Converter, switching and linear regulator reliability figures, the Military Handbook *Reliability Prediction of Electronic Equipment* MIL-HDBK-217F [15] will be used. This handbook provides reliability figures and relationships for various types of electronic components. This will be used as a reference to calculate the overall failure rate, λ, for the buck-boost converter. As shown in (2-12), the MTTF can then also be calculated by considering the overall series system failure rate, λ_S.

In determining the buck-boost converter reliability figure, all components of this building block will be considered as operating in series from the perspective of a structure function – if any listed electronic component fails, then the system itself will be considered as failed and not functioning. Therefore, the series system failure rate, λ_S, is determined by (2-11). The buck-boost converter topology to be considered within this analysis is displayed in **Figure 6,** which is a well-known arrangement. **Table 1** summarizes the parts and quantities for the converter. Only

fundamental circuit elements are considered for this analysis, therefore the MOSFET gate driver is not considered.

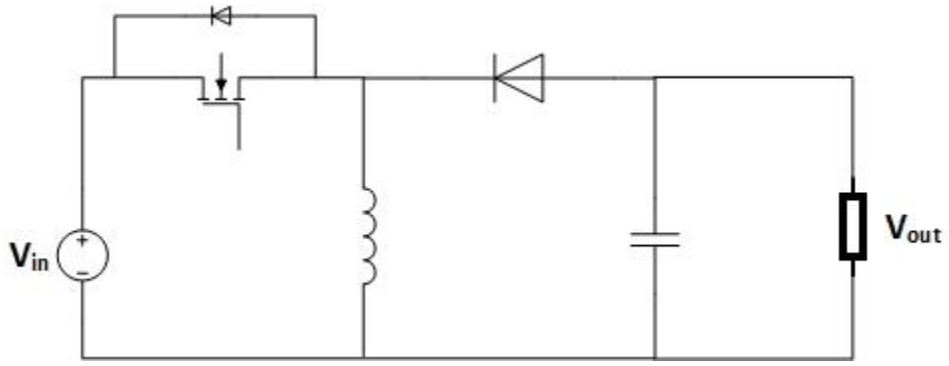

Figure 6—Typical DC-DC Buck-Boost Converter

Table 1—Summary of electrical components in Buck-Boost Converter

Component	Quantity
Diode (Freewheeling and Power)	2
Switching MOSFET	1
Inductor	1
Capacitor	1

To determine the reliability figure of merit for the DC-DC Buck-Boost Converter for this study, the fundamental circuit elements and quantities in **Table 1** are considered each as series elements in the structure function. The MIL Handbook in [15] is used to determine the reliability rates of each component.

2.6.1.1 Freewheeling and Power Diodes

For the freewheeling and power diodes, the same reliability calculation will be considered. According to [15], Section 6.1 – Diodes, Low Frequency, the failure rate can be calculated by

$$\lambda_p = \lambda_b \pi_T \pi_S \pi_C \pi_Q \pi_E \quad \textbf{(2-18)}$$

and is given in Failures/10^6 Hours. **Table 2** summarizes the meaning and value of each variable used in (2-18), as given in [15].

Table 2—Diode failure rate calculation variables

Variable	Meaning	Selected Application	Value
λ_b	Base Failure Rate	Fast recovery power rectifier	0.025
π_T	Temperature Factor	Junction Temperature, T_J = 35 ˚C	1.2
π_S	Electrical Stress Factor	Voltage/Current Regulator	1.0
π_C	Contact Construction Factor	Metallurgically Bonded	1.0
π_Q	Quality Factor	JANTX, unity quality factor	1.0
π_E	Environment Factor	S_F, Space Flight	0.50

The temperature factor, π_T, is individually calculated by first determining the discrete semi-conductor junction temperature, T_J. Given by [15], this is calculated by

$$T_J = T_C + \theta_{JC} P \tag{2-19}$$

where T_C is the component case temperature in °C, θ_{JC} is the junction-to-case thermal resistance in °C/W, and P is the device worst case power dissipation. For space flight, the value of T_C is given as 35°C. An average value of 70 °C/W will be chosen for θ_{JC} (reference Table 6-2 in [15]), and power dissipation, P, can be determined based on typical operating parameters for a power diode used in similar applications. According to [16], a total typical operational load for a CubeSat EPS is roughly 8 Watts at a conservatively calculated current of 2 Amps. Selecting the ON Semiconductor BAV23CL Switching Diode as an example for this analysis, a typical power dissipation for the type of operation described herein is 2.1 mW/°C. Substituting the values of 35°C, 70°C/W, and 0.0021 W/°C for T_C, θ_{JC}, and P, respectively, yields of a value of T_J = 35.147. From Section 6.1 of [15] in the table *Temperature Factor* – π_T, the T_J = 35°C parameter is used, which corresponds a value of π_T = 1.2, which is reflected in **Table 2**.

Substituting the parameters summarized in **Table 2** into (2-18), the failure rate for the freewheeling and power diodes in the DC-DC converter is determined to be λ_p = 0.015 Failures/10^6 hours.

2.6.1.2 Switching MOSFET

The failure rate for the Switching MOSFET of the DC-DC converter displayed in **Figure 6** will be calculated the same way as the freewheeling and power diodes. In [15], Section 6.4 – *Transistor, Low Frequency, Si FET* will be used as the guideline for calculation. This section describes the component under consideration as an "N-Channel and P-Channel Si FET (Frequency ≤ 400 MHz)", which fits the description of the MOSFET to be used in the DC-DC converter. The failure rate, λ_p, given in Failures/10^6 Hours, is given as

$$\lambda_p = \lambda_b \pi_T \pi_A \pi_Q \pi_E \quad \textbf{(2-20)}$$

where **Table 3** summarizes the meaning and values of the parameters used in the equation.

Table 3—MOSFET failure rate calculation variables

Variable	Meaning	Selected Application	Value
λ_b	Base Failure Rate	Transistor Type - MOSFET	0.012
π_T	Temperature Factor	Junction Temperature, T_J = 35 ˚C	1.2
π_A	Application Factor	Power FET, 5 ≤ P_r ≤ 50 Watts	4.0
π_Q	Quality Factor	JANTX, unity quality factor	1.0
π_E	Environment Factor	S_F, Space Flight	0.50

As detailed in **Section 2.6.1.1**, the overall power load of the CubeSAT EPS is roughly 8 W, and therefore an application factor, π_A = 4.0 where the rated power P_r is between 5 and 50 W is used. Further, the same calculation for the temperature factor, π_T, is used, as the devices have similar power ratings and operational characteristics. Substituting the parameters summarized in **Table 3**

into (2-20), the overall failure rate for the switching MOSFET of the DC-DC converter is calculated to be λ_p = 0.0288 Failures/10^6 Hours.

2.6.1.3 Inductor

Again, [15] will be used to determine the reliability rate for the inductor in the DC-DC converter. In the handbook, Section 11.2 – *Inductive Devices, Coils*, will be used as a guideline for calculation. The failure rate for inductors, λ_p, in Failures/10^6 Hours, is then given as

$$\lambda_p = \lambda_b \pi_T \pi_Q \pi_E \quad \textbf{(2-21)}$$

where **Table 4** summarizes the meaning and values of the parameters used in the equation.

Table 4—Inductor failure rate calculation variables

Variable	Meaning	Selected Application	Value
λ_b	Base Failure Rate	Fixed Inductor	0.000030
π_T	Temperature Factor	Hot Spot Temperature, T_{HS} = 30 ˚C	1.1
π_Q	Quality Factor	MIL-SPEC, unity quality factor	1.0
π_E	Environment Factor	S_F, Space Flight	0.50

The temperature factor, π_T, is determined by first calculating the estimated inductor hot spot temperature, T_{HS}. The hot spot temperature, as per [15], is estimated as

$$T_{HS} = T_A + 1.1(\Delta T) \quad \textbf{(2-22)}$$

where T_A is the ambient operating condition and ΔT is the average temperature rise above ambient in ˚C of the inductor during operation. Selecting the Vishay part SGIHLP-48FA-8, which is Space Grade MIL-STD-981 Compliant inductor, and using the selected operating conditions defined earlier of roughly 8 Watts at 2 Amps, the component datasheet specifies, conservatively, a ΔT ˚C above ambient operating conditions of 10˚C. Using a conservative ambient temperature for near-Earth space temperatures of 10˚C [17], T_A = 10˚C, and substituting into (2-22), the inductor hot spot temperature, T_{HS}, is calculated for this application to be 21˚C. Conservatively choosing T_{HS}

= 30°C from the *Temperature Factor-π_T* table in Section 11.2 of [15] yields a temperature factor, π_T, for this analysis of 1.1.

Substituting the parameters summarized in **Table 4** into (2-21), the reliability rate for the DC-DC Converter inductor, λ_p, is calculated to be 16.5 x 10^{-6} Failures/10^6 Hours.

2.6.1.4 Capacitor

Finally, for the last component of the DC-DC Converter, the capacitor, again [15] will be used in the same manner as the MOSFET, diode, and inductor to calculate the reliability rate, λ_p. As per Section 10.1 – *Capacitors* of [15], the relationship to calculate the reliability rate in Failures/10^6 Hours is given as

$$\lambda_p = \lambda_b \pi_T \pi_C \pi_V \pi_{SR} \pi_Q \pi_E \quad \textbf{(2-23)}$$

where **Table 5** summarizes the meaning and values of the parameters used in the equation.

Table 5—Capacitor failure rate calculation variables

Variable	Meaning	Selected Application	Value
λ_b	Base Failure Rate	Capacitor, Fixed, Electrolytic (Solid Electrolyte), Tantalum, Established Reliability	0.00040
π_T	Temperature Factor	Ambient Temperature, T = 20°C	0.91
π_C	Capacitance Factor	C = 18 µF	1.9
π_V	Voltage Stress Factor	CSR 39003 (Column 4 voltage stress factor calculation)	2.0
π_{SR}	Series Resistance Factor	Circuit Resistance, CR = 0.25	2.0
π_Q	Quality Factor	Highest Reliability for Established Reliability Series, Grade D	0.001
π_E	Environment Factor	S_F, Space Flight	0.50

For the purpose of this analysis, a conservatively large value of C = 18 µF is chosen, which is used in determining the capacitance factor, π_C. To determine the voltage stress factor, π_V, the relationship for *Column 4* is Section 10.1 given in [15] must be used:

$$\pi_V = \left(\frac{S}{.6}\right)^{17} + 1 \qquad \textbf{(2-24)}$$

where *S* is the ratio of operating to rated voltage. Choosing a maximum operating voltage of 6V for a capacitor rated at 10V yields $\pi_V = 2.0$.

In determining the series resistance factor, a rough circuit resistance factor must be determined. Choosing a space grade AVX capacitor part number CWR09F^156*@+, the equivalent series resistance of this capacitor is roughly 2.5 Ω at 10 kHz. The circuit resistance, *CR*, is given by [15] as

$$CR = \frac{Effective\ Resistance\ Between\ Cap\ and\ Pwr\ Supply}{Voltage\ Applied\ to\ Capacitor} \qquad \textbf{(2-25)}$$

where the effective resistance between the capacitor and power supply will be assumed to be the Effective Series Resistance given by the AVX datasheet and the voltage applied to the capacitor will be conservatively considered to be 10V. Using these values, a value of $CR = 0.25$ and the corresponding value of π_{SR} is given in the table *Series Resistance Factor* – π_{SR} as 2.0.

The highest quality grade for the Established Reliability series of capacitors, D, was chosen for the quality factor π_Q, which corresponds to a value of 0.001. Capacitors with this quality grade can be selected from the AVX catalog, and will be considered for this study.

Substituting the parameters summarized in **Table 5** into (2-23), the DC-DC Converter capacitor reliability rate, λ_p, is calculated to be 1.38×10^{-6} Failures/10^6 Hours.

2.6.2 DC-DC Converter Component Reliability Summary

Table 6 summarizes the rate of failure of each component in the DC-DC converter used as a building block within the EPS architectures. The component symbols are also summarized in

the table, as they will be used in the calculation to determine the overall rate of failure of the DC-DC converter.

Table 6—Summary of Failure Rates of DC-DC Converter Building Block

Component	Quantity	Failure Rate [Failures/10^6 Hours]	Component Symbol
Diode(s)	2	0.015	λ_D
Switching MOSFET	1	0.0288	λ_{MOS}
Inductor	1	16.5×10^{-6}	λ_L
Capacitor	1	1.38×10^{-6}	λ_C

As discussed previously, the DC-DC converter acts as a system with all of the elements in the structure function, or RBD, in series. This is because if any single item fails, the building block will be considered failed and not functioning as intended. Using (2-10) from **Section 2.3**, the overall rate of failure becomes

$$\lambda_{DC-DC} = \sum_{i=1}^{n} \lambda_i = 2\,\lambda_D + \lambda_{MOS} + \lambda_L + \lambda_C$$
$$= (2)(0.015) + 0.0288 + 0.0000165 + 0.00000138 \quad \textbf{(2-26)}$$
$$= 0.0588\ Failures/10^6\ Hours$$

Using the result from (2-26) and substituting into (2-12) to calculate the MTTF for the DC-DC converter yields

$$MTTF_{DC-DC} = \frac{1}{\lambda_{DC-DC}} = \frac{1}{0.0588} = 17\ x\ 10^6 Hours \quad \textbf{(2-27)}$$

where a $MTTF_{DC\text{-}DC} = 17 \times 10^6$ Hours, or approximately 1,941 Years. Both the DC-DC Converter MTTF and rate of failure are summarized in

Table 7.

Table 7—Summary of Reliability Metrics for the DC-DC Converter Building Block

Reliability Metric	Symbol	Value	Units
Rate of Failure	$\lambda_{DC\text{-}DC}$	0.0588	Failures/10^6 Hours
Mean Time to Failure, MTTF	$MTTF_{DC\text{-}DC}$	17	10^6 Hours

2.6.3 Li-Ion Battery

To calculate the reliability metrics for the Li-Ion Battery Building Block a more straight-forward approach is called for. Due to battery physics, loading, total number of charging and discharging cycles, operational environments, manufacturing quality, and several other factors, precisely determining reliability metrics for a Li-Ion battery for this application becomes quite complicated. Such an analysis can become a dedicated thesis or dissertation in itself, and therefore is out of the scope of this thesis. Detailed statistical failure analysis for Li-Ion batteries can be found in such studies as in [18], however these studies are very much manufacturer dependent, but can lend intuition towards how these components operate.

For the purpose of this thesis, a typical requirement figure for a CubeSat battery will be leveraged. According to [19], an LEO orbit CubeSat has a lifetime requirement, of 2 – 15 years for the deployed battery, or 5 years in average. Such a requirement is typically passed to the battery manufacturer for the specific application. And for the purpose of this thesis, a LEO orbit CubeSat will be considered. In this case, the average lifetime requirement of 5 years will be considered, and therefore the $MTTF_{Battery}$ = 5 Years, or 0.04383 x 10^6 Hours. Rearranging (2-12) to determine the rate of failure

$$\lambda_{Battery} = \frac{1}{MTTF_{Battery}} = \frac{1}{0.04383} = 22.815\ Failures/10^6 Hours \quad \textbf{(2-28)}$$

Clearly, the battery is the lowest reliability item deployed in the EPS architecture for this study. **Table 8** summarizes the Battery Building Block MTTF and failure rate.

Table 8—Summary of Reliability Metrics for the Battery Building Block

Reliability Metric	Symbol	Value	Units
Rate of Failure	$\lambda_{Battery}$	22.815	Failures/10^6 Hours
Mean Time to Failure, MTTF	$MTTF_{Battery}$	0.04383	10^6 Hours

It should be noted here that this is a practical approach to determining the battery reliability. In practice, batteries are on-demand devices, and are only used when necessary and can also fail when not being used. As discussed in the description of the baseline architecture, a battery is used to provide energy during eclipse cycles when solar energy is not readily available. Solar energy could also be unavailable during periods when the CubeSat is not properly oriented towards the sun as well. Therefore, battery on-demand usage is very unpredictable. Since the availability of solar energy is also unpredictable during certain circumstances, the charging and discharging cycles of the employed batteries are very difficult to determine. All of these factors impact the overall reliability of the battery and for an accurate representation of both the operation and reliability of the battery, more complex modeling would be required. Further, for reliability modeling of batteries, Markov chains are typically employed. A Markov chain is a stochastic model utilizing probability functions to determine the reliability of a component, and is a good tool for modeling battery system reliability. Such an approach is out of the scope of this thesis and not necessary to meet the intent of this analysis.

2.6.4 PV Array

Another straight-forward approach will be taken for determining the Building Block reliability metric for the PV Arrays installed in the CubeSat. As mentioned in Section 1.0, five PV panels are typically wired in series, generally to increase the overall voltage output of the array [11]. As will be introduced in the next chapter, this array of panels will be split out in various configurations throughout the proposed EPS architectures. It is assumed within this comparative analysis that under certain circumstances and distributed loading, that a single PV panel can properly provide the required energy for the load it is ultimately feeding. In these cases, a dedicated DC-DC boost converter will be provided to the individual panel and will be capable of regulating the voltage as required and will be equipped with MPPT capabilities. Again, this will be discussed in the next chapter.

However, a reliability metric must still be determined for the comparative analysis. The MIL Handbook used in calculating the reliability metrics for the DC-DC converter cannot be used here, as it does not present data relevant for determining photovoltaic failure rates. For the purpose of this study, consumer data for residential installations of PV arrays will be leveraged. Since the purpose of this thesis is a comparative analysis between a baseline and proposed architectures, all data used between the various configurations will be equal. There is no proposal to change technology between configurations; only to reconfigure in various manners. Therefore, a solid reliability metric based on real-world data will be sufficient for use in this study.

According to [20], out of residential PV installations between 2000 and 2015, a median failure rate was observed of 5 panels out of 10,000 annually, which corresponds to 5 failures per 87.7×10^6 Hours, or a $MTTF_{PV} = 1.7532 \times 10^6$ Hours. Rearranging (2-12) to calculate the failure rate yields

$$\lambda_{PV} = \frac{1}{MTTF_{PV}} = \frac{1}{17.532} = 0.0570\ Failures/10^6 Hours \quad \textbf{(2-29)}$$

Table 9 summarizes the individual PV panel MTTF and failure rate.

Table 9—Summary of Reliability Metrics for PV Building Block

Reliability Metric	Symbol	Value	Units
Rate of Failure	λ_{PV}	0.0570	Failures/10^6 Hours
Mean Time to Failure, MTTF	$MTTF_{PV}$	17.532	10^6 Hours

2.6.5 Summary of Building Block Reliability Metrics and Final Approach

As calculated in the preceding sections, **Table 10** summarizes all of the reliability metrics quantifying the various Building Blocks described earlier. This table will be referenced throughout the analysis and used in calculation to quantify the reliability figure for each proposed architecture EPS. These metrics will be used in conjunction with the RBD determined for each proposed architecture. Parallel structures will be reduced to a single element using the relationships described earlier. The resulting series elements in the RBD will be combined to determine a single failure rate and MTTF metric for each EPS. Ultimately, these metrics will be used to compare the viability of each architecture and to rank them accordingly.

Table 10—Summary of Reliability Metrics for Building Blocks

Reliability Metric	DC-DC Converter	Li-Ion Battery	PV Panel
Rate of Failure [Failures/10^6 Hours]	0.0588	22.815	0.0570
Mean Time to Failure, MTTF [10^6 Hours]	17	0.0438	17.532

3.0 Electric Power System Architectures and Comparisons

As mentioned in Chapter 1.0, ten EPS architectures will be compared to a baseline architecture, which has already been introduced and is displayed as **Figure 1**. The baseline architecture will act as the primary point of comparison against all subsequent variations. Further, the variations will be compared against one another, ultimately ranking and stacking the reliability metrics. This will lead to a conclusion as to which architectures may be the most suitable for future research and development.

The goal of each architecture is to improve upon the reliability metrics determined for the baseline architecture. The goal of this chapter is to introduce each alternative background and give an overview of how it differs from the baseline architecture.

3.1 Nomenclature and Symbols

In order to effectively develop symbolic EPS architectures and corresponding RBDs, nomenclature must be developed. Each Building Block deployed will have a corresponding element number. For example, if four DC-DC Boost converters are used in a specific architecture, they will be labeled Cc_1, Cc_2, Cc_3, and Cc_4. Each element in an architecture will have an independent identifier so all components can be accounted for. **Table 11** summarizes the nomenclature to be used throughout this analysis. For each symbol, the subscript '*i*' indicates the element number of that specific Build Block.

Table 11—Nomenclature for Building Blocks

Building Block/Component	Symbol
PV Panel (Fuel Source)	F_i
DC-DC Boost Converter w/ MPPT	Cc_i
Li-Ion Battery (Energy Source)	Es_i
Load DC-DC Converter	Cr_i

3.2 Architecture #1 – Distributed Battery Power

Proposed EPS Architecture #1 is displayed as **Figure 7**. In this architecture, batteries are added from the baseline and dedicated to each load DC-DC converter. Because of this addition, the bi-directional converter from the baseline is removed, as it is no longer necessary, as each battery will be independently driven by the load DC-DC converters. The five-sided PV array, labeled as $f_{1\text{-}5}$, remains as it was in the baseline. The total component count for this architecture is 14.

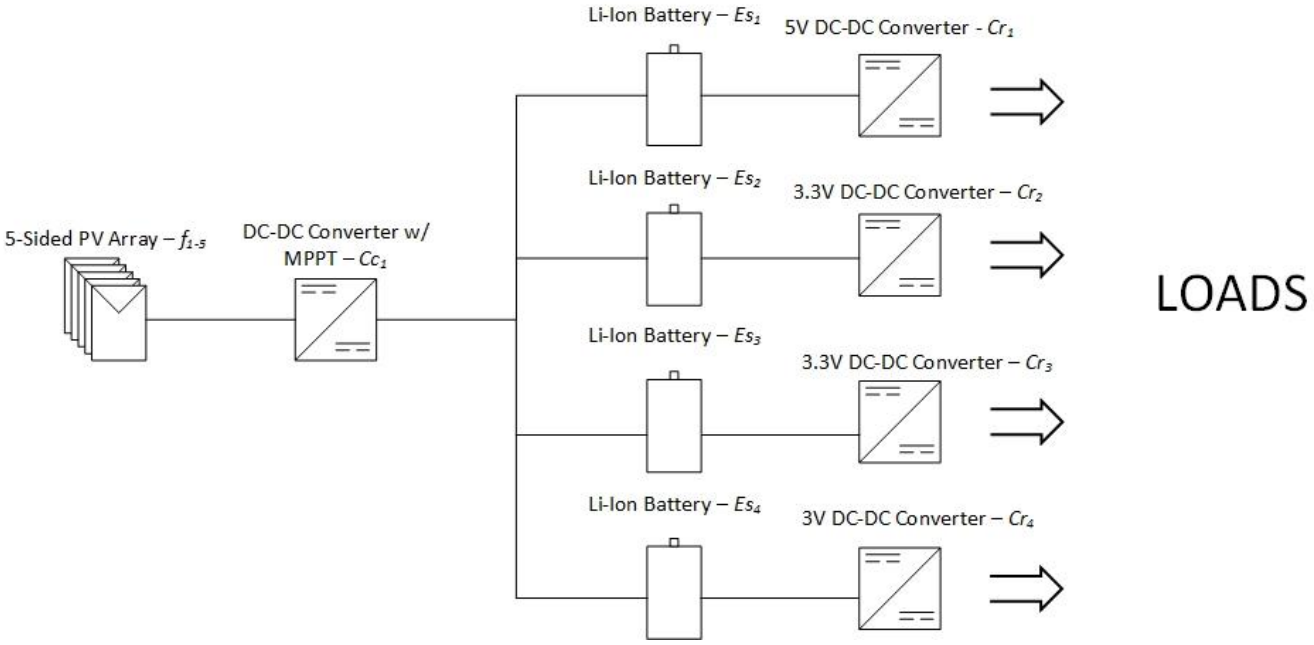

Figure 7—Architecture #1

3.3 Architecture #2 – Distributed Battery Power with Redundant 3.3V Output

Proposed EPS Architecture #2 is displayed as **Figure 8**. This architecture is very similar to Architecture #1, with one key difference – the DC Link for converters Cr_2 and Cr_3 are now shared. This serves a few different purposes that aid in improving the overall architecture reliability from Architecture #1. First, it provides parallel redundancy for the 3.3V loads. If either Cr_2 or Cr_3 fails, the other will continue to provide power for the 3.3V loads. It is assumed that the DC-DC converters are sized such that they can handle the increased load in such a scenario. Second, it also provides redundancy if battery Es_2 or Es_3 fails. While a battery failure would render the associated DC-DC Converter inoperable, the parallel converter can account for this failure mode. In such scenarios as described, whether a DC-DC converter or battery fails, that section of the electrical circuit would no longer draw any load and energy would load balance to the remaining components accordingly. The five-sided PV array, labeled as $f_{1\text{-}5}$, remains as it was in the baseline. The total component count for this architecture remains at 14.

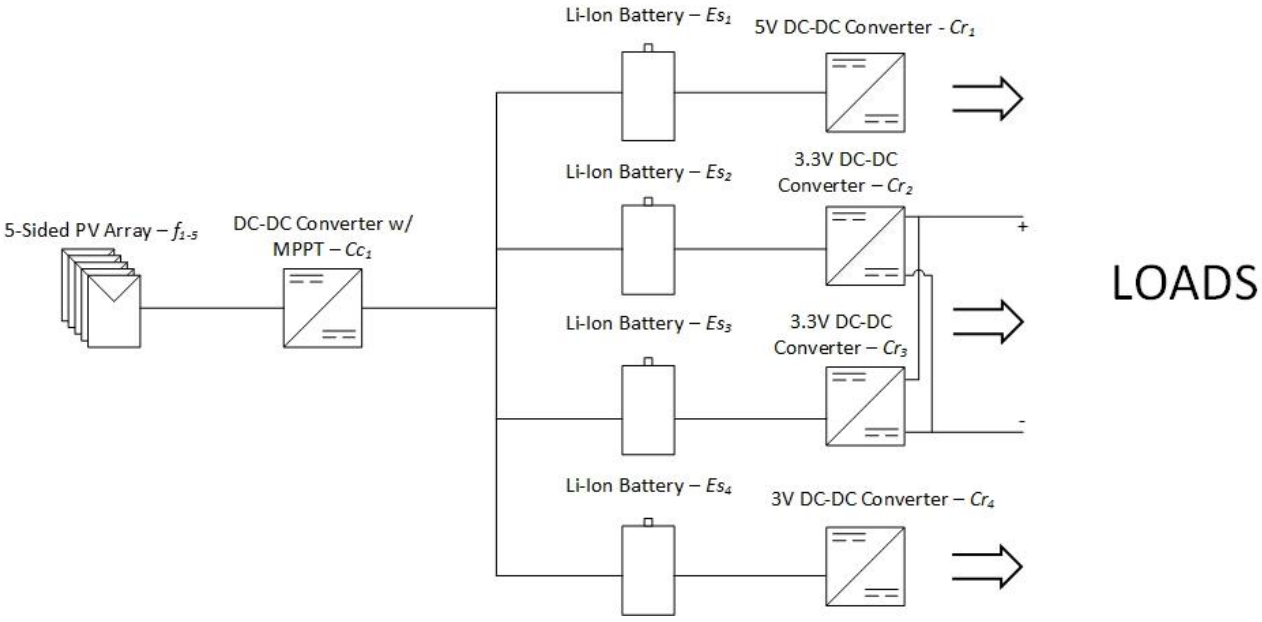

Figure 8—Architecture #2

3.4 Architecture #3 – Fully Distributed Load Chains

Proposed EPS Architecture #3 is displayed as **Figure 9**. This is a distributed architecture, where all load chains are broken out into independent circuits within the architecture. Between different load circuits (e.g., 5V, 3.3V, 3V), there are no shared components. While this style architecture will not likely improve the reliability from the baseline, it does provide that if any components in one chain fail, the rest of the system can remain operational, granted the load is not critical in continuing the CubeSat mission. Each PV panel is dedicated to a load chain, where the additional panel is configured in series for the 5V circuit. The total number of components for this architecture increases to 17.

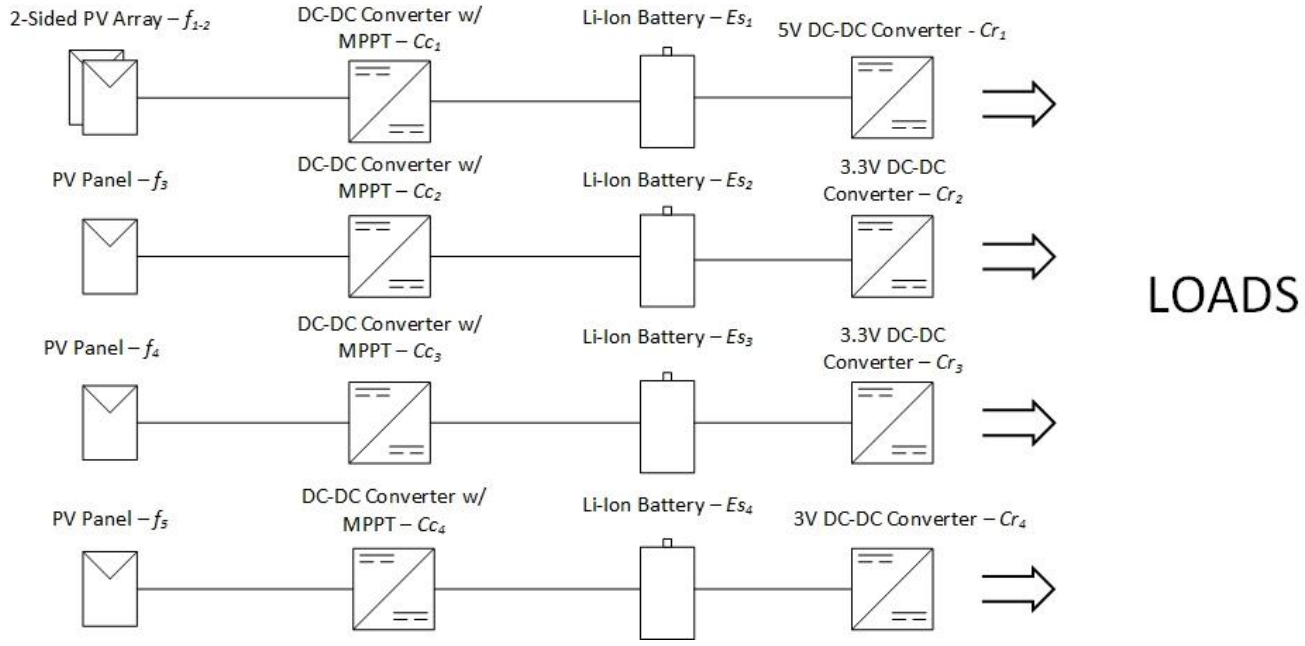

Figure 9—Architecture #3

3.5 Architecture #4 – Fully Distributed Load Chains with Redundant 3.3V Output

Proposed EPS Architecture #4 is displayed as **Figure 10**. This architecture is nearly identical to the previous architecture, Architecture #3, but with one difference – the output of the two 3.3V DC-DC converter DC Links are tied together, similar to Architecture #2. Again, the advantage here is the redundancy of both DC-DC Converters for each load chain as well as the redundancy of the Li-Ion batteries. This too is a distributed architecture, where all load chains are broken out into independent circuits within the architecture but the 3.3V load chain has the advantage of redundancy. This style architecture may improve upon the reliability from the baseline. Further, if one load chain does cease to function, the rest of the system can remain operational as explained before, granted the lost load capability is not critical in continuing the CubeSat mission. Each PV panel is dedicated to a load chain, where the additional panel is configured in series for the 5V circuit. The total number of components for this architecture remains at 17.

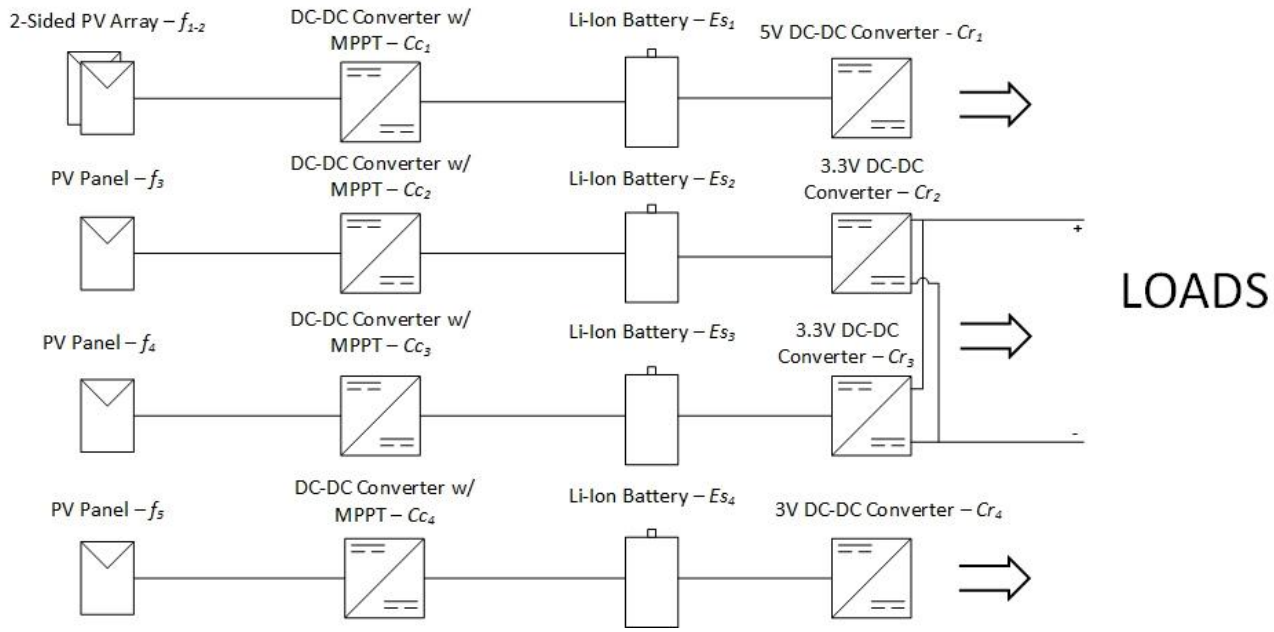

Figure 10—Architecture #4

3.6 Architecture #5 – Fully Distributed Load Chains with Common PV Bus

Proposed EPS Architecture #5 is displayed as **Figure 11**. Architecture #5 builds on the concepts of Architectures #3 and #4. It is a distributed architecture, combines the outputs of the 3.3V DC-DC Load converters, and also reconfigures the PV panels to form a parallel array, as to provide further redundancy of the primary energy source. By reconfiguring the PV array, a large amount of redundancy is introduced. Further, by introducing independent DC-DC Boost Converters with MPPT for each PV panel, it is assumed that the parallel configuration is technically feasible. A low voltage bus can be formed through the parallel arrangement of all PV panels and active load balancing of such an arrangement similar to as proposed in [22] may be a feasible technical solution for implementation. In the case of Architecture #5, each DC-DC Boost Converter can be used for PV cell balancing, while the arrangement can provide for a high level of redundancy. It is likely this architecture will improve upon Architectures #3 and #4, and may improve upon the reliability of the baseline architecture and provide more flexibility to the overall system designer. The total number of components for this configuration remains at 17.

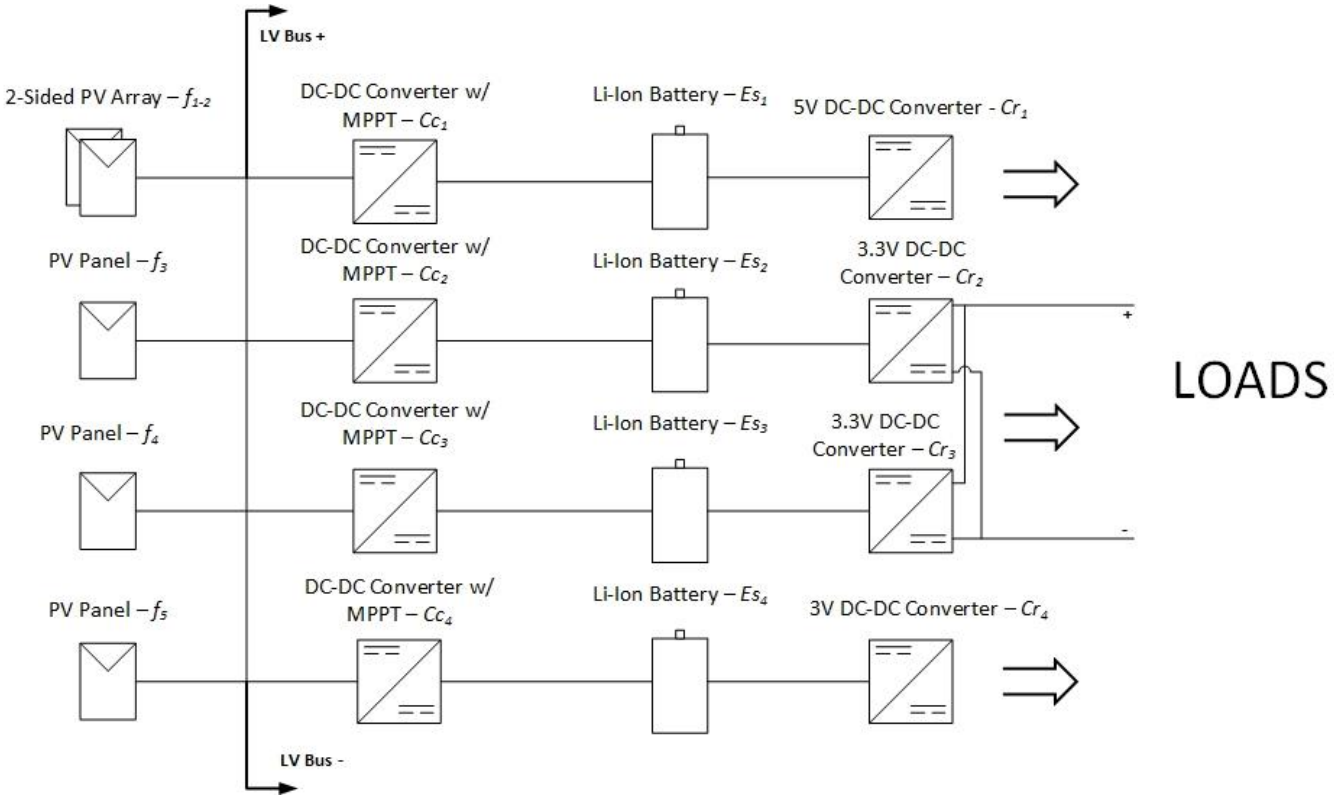

Figure 11—Architecture #5

3.7 Architecture #6 – Fully Distributed with Common 3.3V Load Chain

Proposed EPS Architecture #6 is displayed as **Figure 12**. Architecture #6 is similar to #5, however the full redundancy of the PV panels configured in parallel is partially removed from this topology. Only for the 3.3V load chain is this particular configuration preserved. The reasoning for this is based on both technical feasibility and to improve the redundancy of the 3.3V load chain. It may be beneficial to look at the improvement to reliability above the baseline of this architecture if the configuration described in Architecture #5 cannot reliably be developed. The total number of components for this configuration remains at 17.

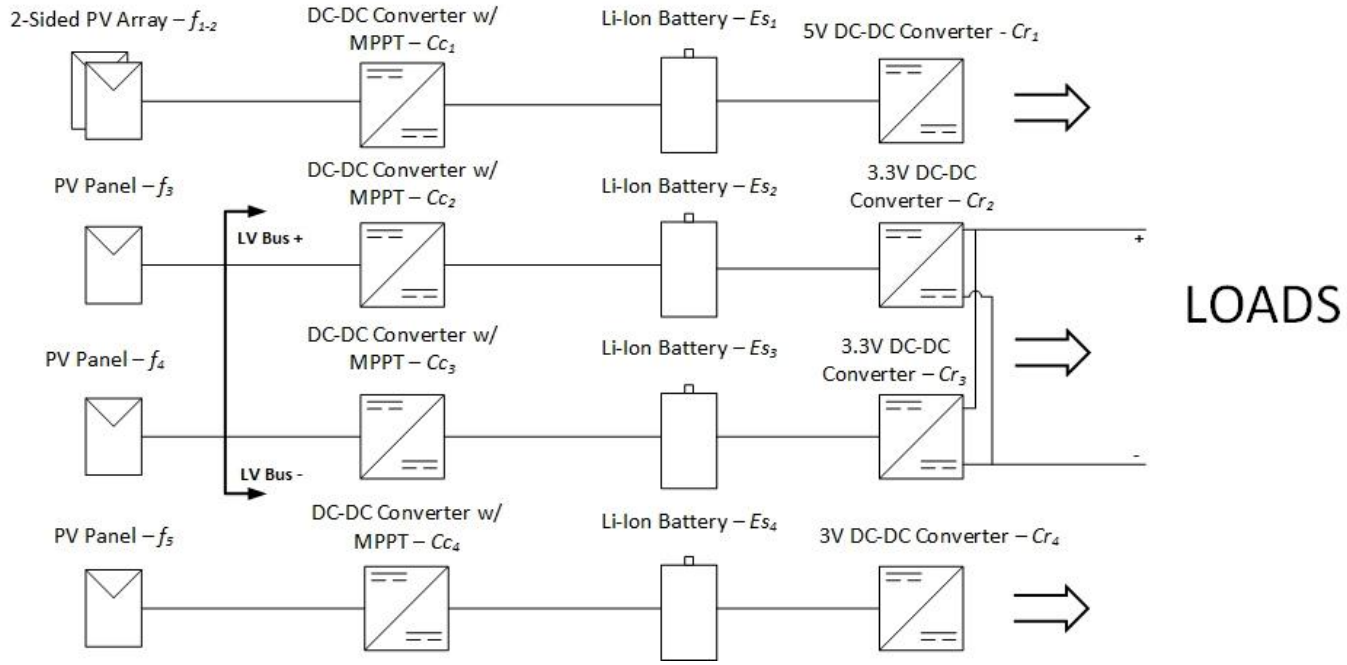

Figure 12—Architecture #6

3.8 Architecture #7 – Fully Distributed with Common PV Bus and Redundant 3.3V Output

Proposed EPS Architecture #7 is displayed as **Figure 13**. Architecture #7 builds on #5 and adds an element of redundancy for the Li-Ion batteries in the 3.3VDC load chain. Since this load chain is already sharing the redundancy for the DC-DC Load Converters, it follows that the energy source, the two Li-Ion batteries, should be shared in a redundant manner as well. This adds redundancy on another level opposed to prior architectures—while a failure of a Li-Ion battery in the 3.3VD load chain in Architecture #2 could fail, for example, this type of failure would not preclude disabling its associated DC-DC Load Converter. In this architecture, a battery could fail and power could be re-routed through the opposite DC-DC Load Converter in the chain, however the failed battery would then render its corresponding DC-DC Load Converter non-functional. With the topology arranged as such in Architecture #7, this type of failure mode will not exist. Therefore, it will be critical to compare the benefits in the reliability metrics of Architecture #7 to previously detailed architectures. It is assumed that this architecture is designed such that the batteries for the 3.3VDC load chains are not able to discharge into one another. The number of components for this configuration remains at 17.

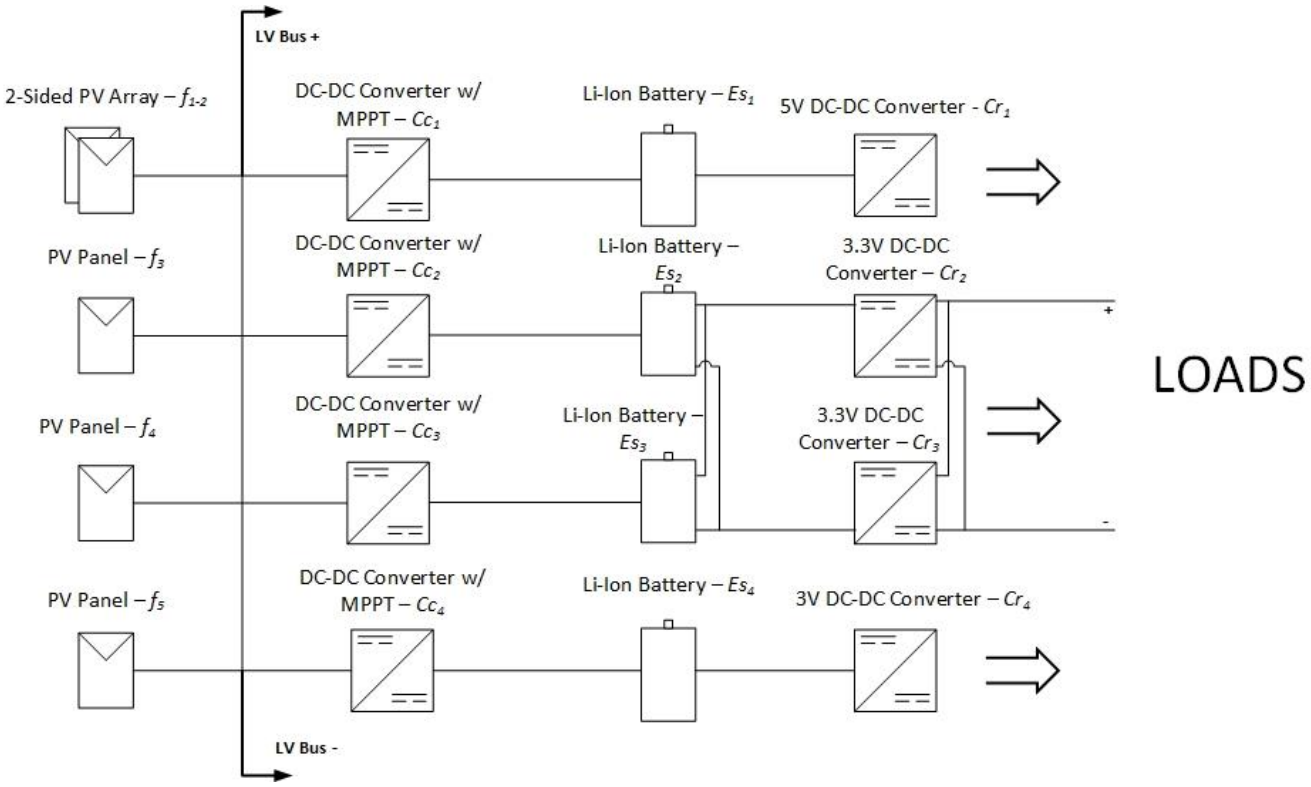

Figure 13—Architecture #7

3.9 Architecture #8 – Fully Distributed with Common Battery Bus and Redundant 3.3V Output

Proposed EPS Architecture #8 is displayed as **Figure 14**. Architecture #8 builds on all previously discussed architectures by adding redundancy in a similar manner. In this configuration, the LV parallel bus redundancy is implemented across the Li-Ion battery building blocks. Again, it is assumed this is a feasible technical solution that can be implemented in a similar manner as in [22]. However, the low voltage bus redundancy is removed from the PV Panel Array building blocks. With this architecture, an improvement to the baseline is expected, as the least reliable component, the Li-Ion battery, now has a very high level of redundancy. By removing the LV Bus across the PV Array building blocks, the impact of battery redundancy can more clearly be determined. The number of components for this configuration remains at 17.

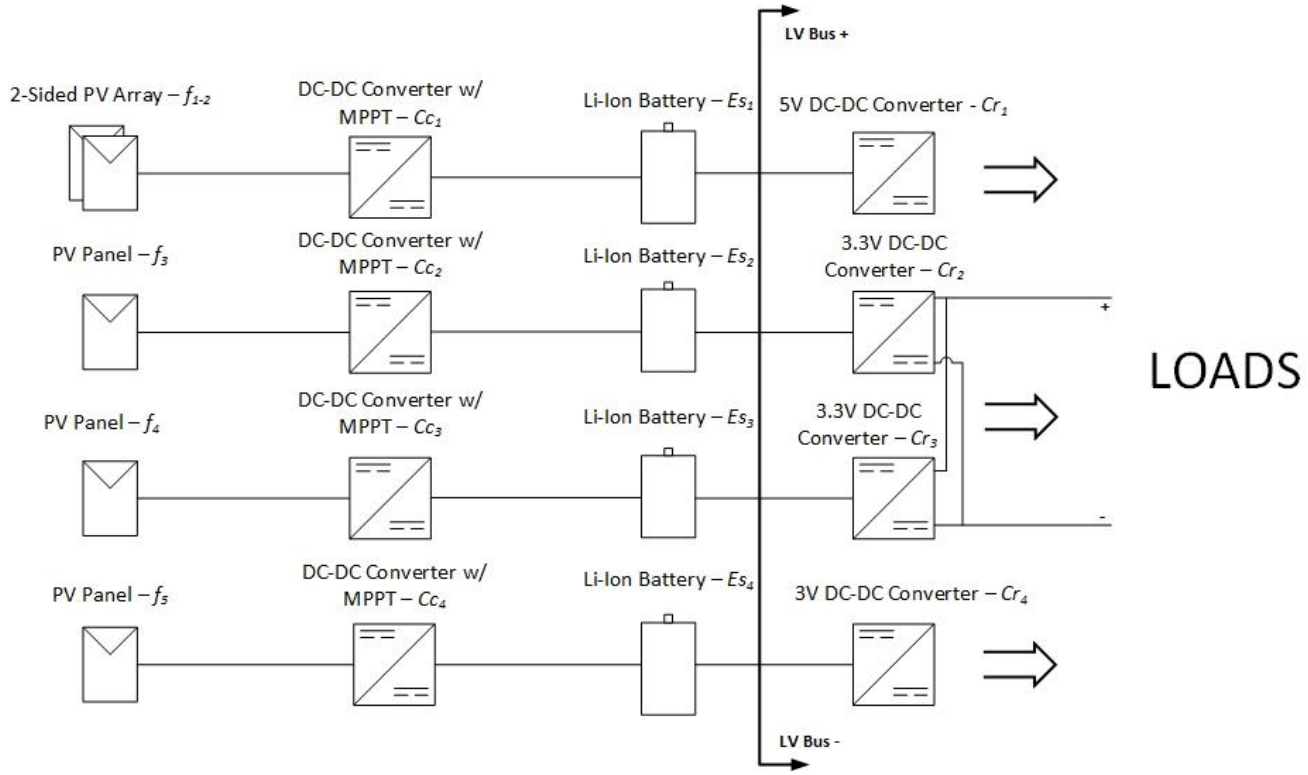

Figure 14—Architecture #8

3.10 Architecture #9 – Fully Distributed with Common PV Bus and Common Battery Bus

Proposed EPS Architecture #9 is displayed as **Figure 15**. Architecture #9 builds on Architectures #7 and #8 by implementing the Low Voltage bus on both the PV Array bank and the Li-Ion battery bank. By implementing the Low Voltage bus in this manner, a high amount of redundancy becomes available of both the fuel source (PV Array) and energy source (Li-Ion battery) building blocks. The 3.3VDC load output converters are tied together with a common DC link just as Architectures #4 - #8 are. It is expected that this topology affords the highest reliability above the baseline. Again, it is assumed that topology is properly load balanced that this architecture is technically feasible. The number of components for this configuration remains at 17.

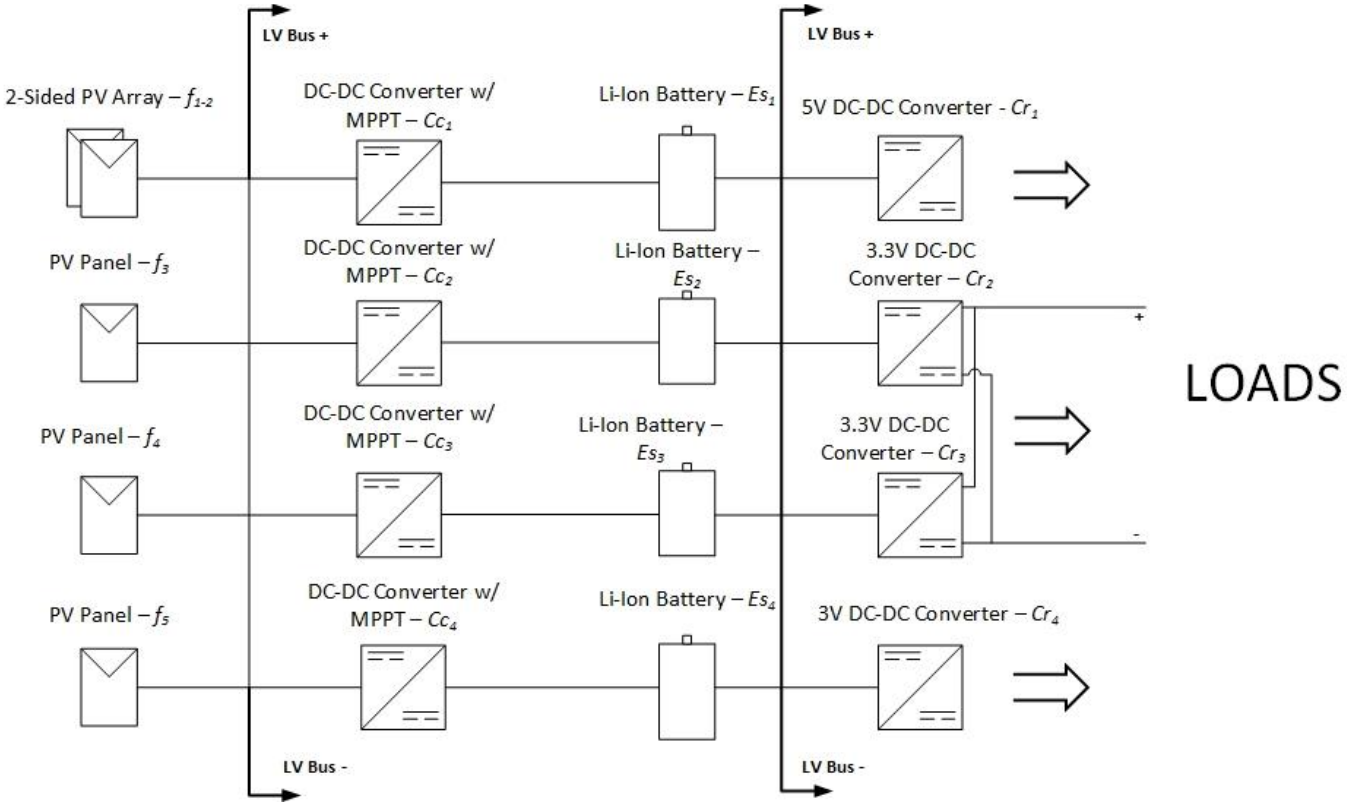

Figure 15—Architecture #9

3.11 Architecture #10 – Fully Distributed with Common PV Bus, DC-DC Converter Output Bus, and Battery Bus

Architecture #10 is the final proposed EPS architecture and is displayed as **Figure 16**. This architecture combines all the elements of redundancy introduced in prior architectures: the fuel source LV bus, energy source LV bus, and the common DC link on the 3.3VDC load chain. Further, another LV bus is added to the output of the DC-DC Boost Converters. For this topology, nearly every component now has an element of redundancy introduced. In the case of any redundant element that fails, it is assumed that the proper load balancing is integrated within the system to handle the power flow throughout the EPS. It is expected that this topology will afford the highest reliability above the baseline while still maintaining the same number of components, 17, as the previous architectures.

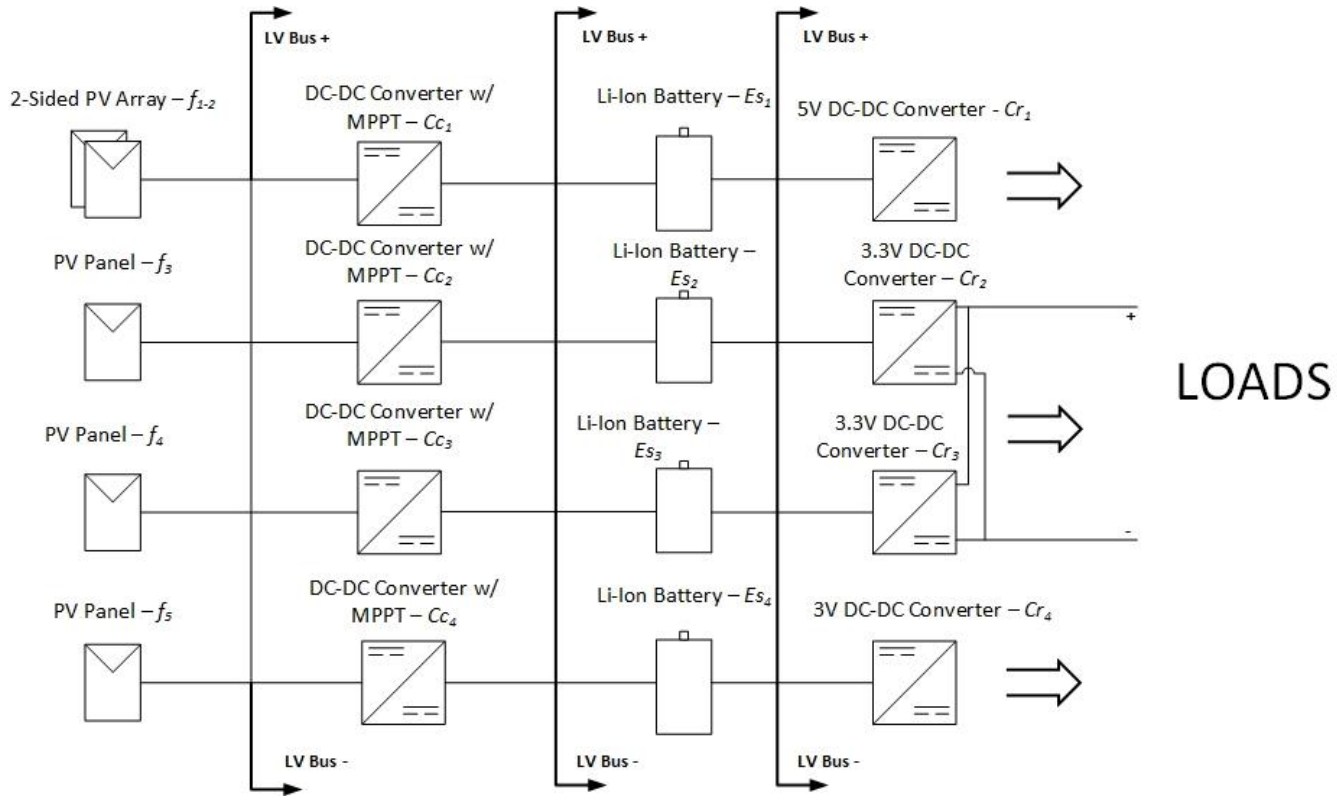

Figure 16—Architecture #10

To illustrate the concept of redundancy in Architecture #10, consider **Figure 17**. In this illustration, the Li-Ion battery for the 5VDC load chain, Es_1, fails. The figure shows the redirection of power flow through the rest of architecture around the battery and back to the 5VDC load converter, Cr_1. This re-routed power flow highlights the power and importance of introducing redundancy into the EPS architecture. Power flow beyond the DC-DC Boost Converters, Cc_i, is illustrated.

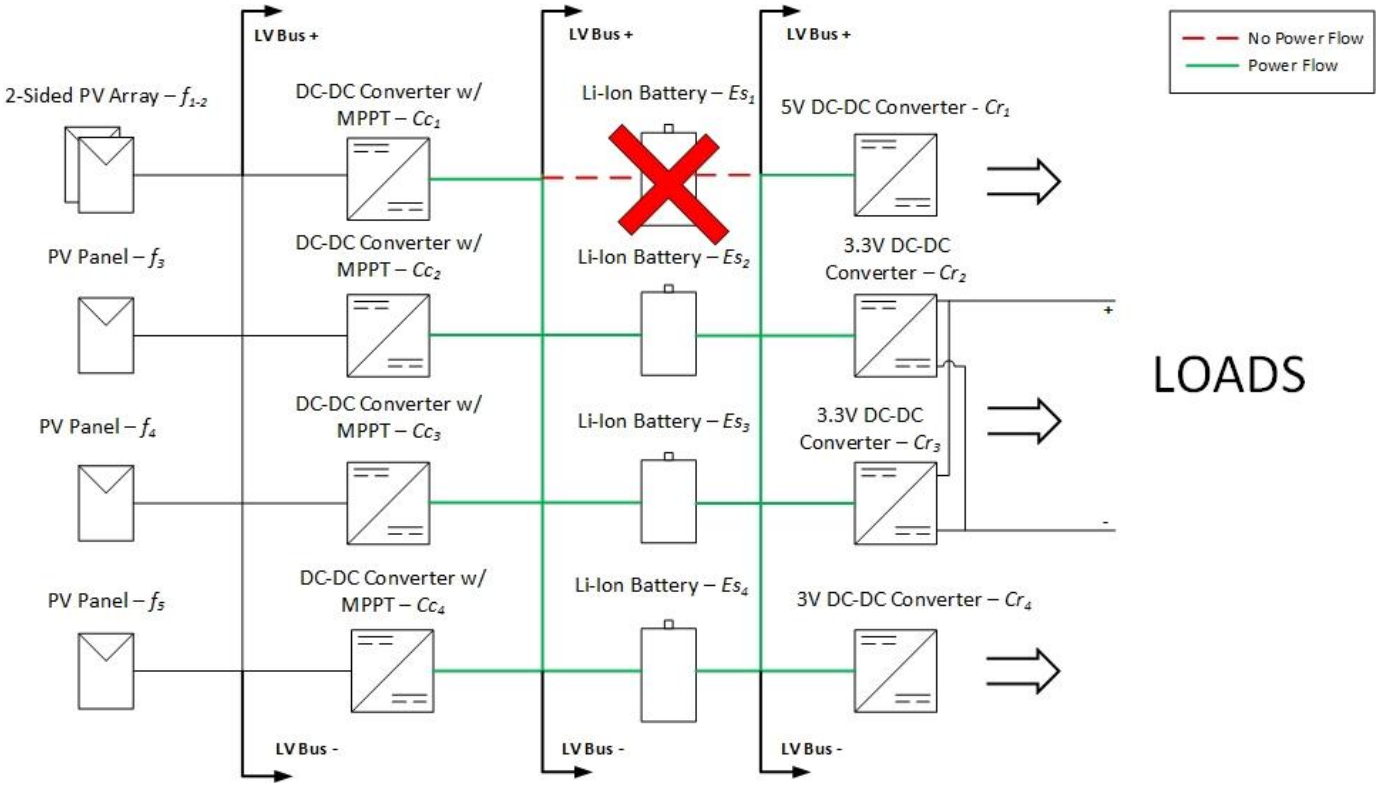

Figure 17—Redirected power flow during Es_1 failure in Architecture #10

3.12 Summary of Electric Power System Architecture Proposals

Table 12 provides a summary overview of the ten proposed EPS architectures as well as the baseline. These architectures are not ranked; they are simply numbered from the baseline to Architecture #10. The total number of components, broken out by Building Block, is included.

Table 12—Summary of EPS Architectures

	Number of Building Block Components						
Architecture	**PV Panels - f_i**	**DC-DC Boost Converter - Co_i**	**Li-Ion Battery - Es_i**	**Load Converter - Cr_i**	**Total Number of Components**	**Reference Figure**	**Brief Description of Architecture**
Traditional Architecture (Baseline)	5	2	1	4	12	Figure 1	Architecture which others will be compared against.
Architecture #1	5	1	4	4	14	Figure 7	Distributed architecture with no redundancy and single DC-DC Boost Converter.
Architecture #2	5	1	4	4	14	Figure 8	Distributed architecture with redundancy on 3.3V load output. Single DC-DC Boost Converter implementation.
Architecture #3	5	4	4	4	17	Figure 9	Distributed architecture with no redundancy but with distributed DC-DC Boost Converters.
Architecture #4	5	4	4	4	17	Figure 10	Distributed architecture with redundancy on 3.3V load output. Distributed DC-DC Boost Converters.
Architecture #5	5	4	4	4	17	Figure 11	Distributed architecture with PV Panel LV Bus introduced for redundancy. 3.3V load output redundancy.
Architecture #6	5	4	4	4	17	Figure 12	Distributed architecture with PV Panel redundancy on 3.3V load chain. 3.3V load output redundancy.
Architecture #7	5	4	4	4	17	Figure 13	Distributed architecture with PV Panel LV Bus for fuel source redundancy. Redundancy of 3.3V load chain Li-Ion batteries and output converters.
Architecture #8	5	4	4	4	17	Figure 14	Distributed architecture with redundancy on entire Li-Ion battery bus. 3.3V load output redundancy.
Architecture #9	5	4	4	4	17	Figure 15	LV Bus redundancy on PV Panel and Li-Ion battery buses. 3.3V load output redundancy.
Architecture #10	5	4	4	4	17	Figure 16	Redundancy introduced by LV bus on PV Panel Array, DC-DC Boost Converter output, and Li-Ion Batteries. 3.3V load output redundancy.

4.0 Minimal Cut Sets, Reliability Block Diagrams, and Reliability Analysis for Each EPS Architecture

With *Chapter 4.0*, the minimal cut sets, RBDs, and reliability analysis will be presented for the baseline architecture and the ten alternative architectures presented previously. Minimal cut sets are defined as explained in *Chapter 2.5 - Minimal Cut Sets*. Using the minimal cut sets, the RBD for each architecture can easily be developed. Once the RBD is developed for an architecture, the structure function can easily be determined. From the structure function, parallel and series combinations of RBD elements can be combined to determine both an overall failure rate, λ, and MTTF. Parallel elements are to be reduced as outlined in *Chapter 2.0* and then easily combined with other series elements, leading to the overall system reliability figure.

The reliability metrics summarized for each Building Block in **Table 10** from *Chapter 2.0* will be presented within each element of the RBD for easy reference. The metric to be presented directly on the element will be the failure rate, λ. The structure function will be determined using the failure rate and the overall reliability metric for the system will be converted to MTTF as per Equation (2-12) once the entire system is broken down into only series elements.

Minimal cut sets will be presented in curly brackets (braces) that enclose an entire cut set. All elements within a brace represent a group of elements that are a parallel cut set. Cut sets that are similar in nature will be separated by a comma in the minimal cut set table.

4.1 Traditional Architecture (Baseline)

The traditional architecture, presented in **Figure 1**, is relatively straightforward in terms of analysis. All elements within this baseline architecture are single points of failure. If one single element fails, this entire architecture is no longer functional. Therefore, the minimal cut sets are simply every element, of which there are 12, individually listed. The minimal cut sets are summarized in **Table 13**. In developing these cut sets, it assumed that even if the battery has a full charge and the PV Array or DC-DC boost converter fails, that the system for all intents and purposes is now failed and cannot function as originally intended.

Table 13—Traditional Architecture (Baseline) Minimal Cut Sets

Minimal Cut Set #	Minimal Cut Sets	Cut Set Description
1	$\{f_1\}, \{f_2\}, \{f_3\}, \{f_4\}, \{f_5\}$	Fuel Source - PV Array
2	$\{Cc_1\}$	DC-DC Boost Converter
3	$\{Cc_2\}$	Bi-directional DC-DC Battery Converter
4	$\{Cr_1\}$	5V Load Converter
5	$\{Cr_2\}$	3.3V Load Converter #1
6	$\{Cr_3\}$	3.3V Load Converter #2
7	$\{Cr_4\}$	3V Load Converter
8	$\{Es_1\}$	Li-Ion Battery

Using the minimal cut sets, the RBD for the traditional architecture is developed and is displayed as **Figure 18**.

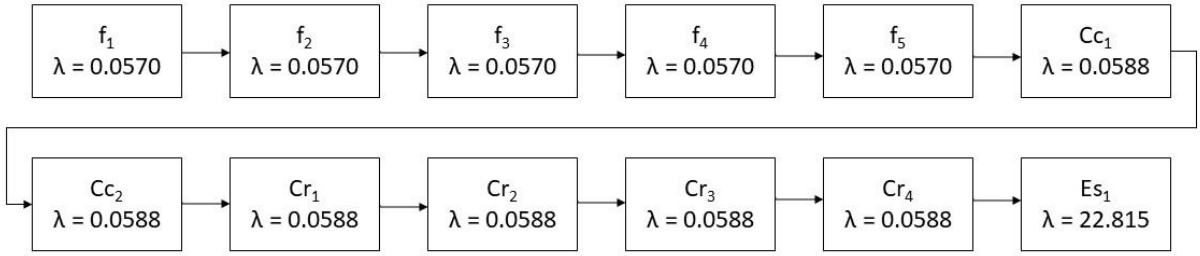

Figure 18—Traditional Architecture (Baseline) RBD

Using the relationship to calculate the overall system failure rate in (2-10), the traditional architecture (baseline) failure rate relationship is given by

$$\lambda_{Baseline} = \lambda_{f_1} + \lambda_{f_2} + \lambda_{f_3} + \lambda_{f_4} + \lambda_{f_5} + \lambda_{Cc_1} + \lambda_{Cc_2} + \lambda_{Cr_1} + \lambda_{Cr_2} + \lambda_{Cr_3} + \lambda_{Cr_4} + \lambda_{Es_1} = 23.453 \frac{Failures}{10^6\ Hours} \quad \textbf{(3-1)}$$

and using (2-12) to determine the MTTF yields

$$MTTF_{Baseline} = \frac{1}{\lambda_{Baseline}} = \frac{1}{23.453} = 0.0426\ x\ 10^6 Hours \quad \textbf{(3-2)}$$

An MTTF of 0.0426 x 10^6 Hours equals 4.864 years, where there is 8,766 hours per year on average. It is expected that the MTTF for the baseline architecture is less than 5 years, considering the lifetime expectancy of the Li-Ion battery building block outlined in *Chapter 2.6.3.*

4.2 Architecture #1

Architecture #1 was presented earlier as **Figure 7**. This architecture does not add any elements of redundancy or aspects that conceivably could improve upon the baseline architecture reliability metric. As discussed, this EPS breaks out elements to form a distributed architecture, however all elements are single points of failure. Again, the minimal cut sets for this architecture are simply every element broken out, similar to the baseline architecture. The minimal cut sets for this architecture are summarized in **Table 14**.

Table 14—Architecture #1 Minimal Cut Sets

Minimal Cut Set #	Minimal Cut Sets	Cut Set Description
1	$\{f_1\}, \{f_2\}, \{f_3\}, \{f_4\}, \{f_5\}$	Fuel Source - PV Array
2	$\{Cc_1\}$	DC-DC Boost Converter
3	$\{Es_1\}$	Li-Ion Battery
4	$\{Es_2\}$	Li-Ion Battery
5	$\{Es_3\}$	Li-Ion Battery
6	$\{Es_4\}$	Li-Ion Battery
7	$\{Cr_1\}$	5V Load Converter
8	$\{Cr_2\}$	3.3V Load Converter #1
9	$\{Cr_3\}$	3.3V Load Converter #2
10	$\{Cr_4\}$	3V Load Converter

Similar to the baseline architecture, the RBD for Architecture #1 is simply all elements in series and is displayed as **Figure 19**.

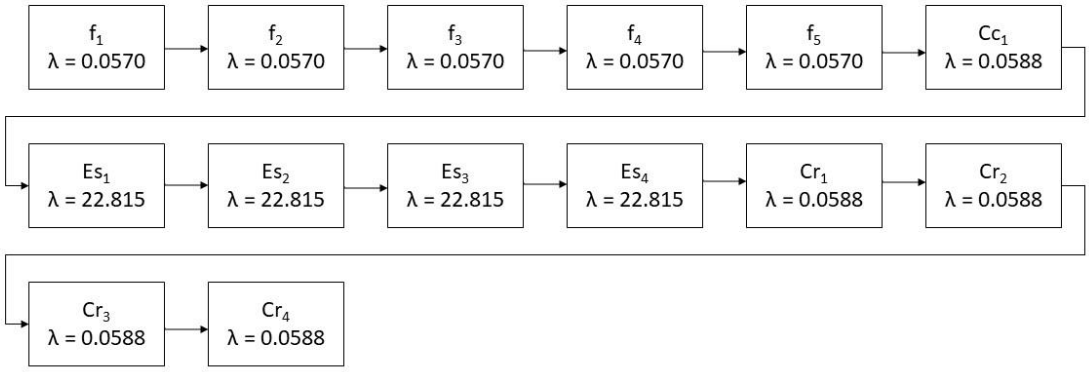

Figure 19—Architecture #1 RBD

Again using the simple relationship to calculate the overall system failure rate in (2-10), the failure rate relationship for Architecture #1 is given as

$$\lambda_{Arch\#1} = \lambda_{f_1} + \lambda_{f_2} + \lambda_{f_3} + \lambda_{f_4} + \lambda_{f_5} + \lambda_{Cc_1} + \lambda_{Es_1} + \lambda_{Es_2} + \lambda_{Es_3} + \lambda_{Es_4} + \lambda_{Cr_1} + \lambda_{Cr_2} + \lambda_{Cr_3} + \lambda_{Cr_4} = 91.839 \frac{Failures}{10^6\ Hours} \quad \textbf{(3-3)}$$

and using (2-12) to determine the MTTF yields

$$MTTF_{Arch\#1} = \frac{1}{\lambda_{Arch\#1}} = \frac{1}{91.839} = 0.0109\ x\ 10^6 Hours \quad \textbf{(3-4)}$$

An MTTF of 0.0109 x 10^6 Hours equals 1.242 years. As expected, by introducing 3 additional Li-Ion batteries into the architecture in a non-redundant fashion severely impacts the overall reliability metric in a negative way relative to the baseline for Architecture #1.

4.3 Architecture #2

Architecture #2 was presented as **Figure 8**. Architecture #2 introduces the first element of redundancy by tying the 3.3V load chain load converter DC Links together in a parallel fashion. The rest of the EPS architecture remains the same as Architecture #1. Even though it is a single element of redundancy at the 3.3V output converters, another level of redundancy opens up for this system for the battery building block. For example, if a Li-Ion battery fails in one 3.3V load chain, the other load chain will compensate and still provide the 3.3V output. This should increase the reliability from Architecture #1, but not likely increase the reliability from the baseline. The minimal cut sets for Architecture #2 are summarized in **Table 15**.

Table 15—Architecture #2 Minimal Cut Sets

Minimal Cut Set #	Minimal Cut Sets	Cut Set Description
1	$\{f_1\}, \{f_2\}, \{f_3\}, \{f_4\}, \{f_5\}$	Fuel Source - PV Array
2	$\{Cc_1\}$	DC-DC Boost Converter
3	$\{Es_1\}$	Li-Ion Battery
4	$\{Es_2, Cr_3\}$	Li-Ion Battery and 3.3V Load Converter in adjacent load chains.
5	$\{Es_3, Cr_2\}$	Li-Ion Battery and 3.3V Load Converter in adjacent load chains.
6	$\{Es_4\}$	Li-Ion Battery
7	$\{Cr_1\}$	5V Load Converter
8	$\{Cr_2, Cr_3\}$	3.3V Load Converters
9	$\{Es_2, Es_3\}$	Li-Ion Batteries in 3.3V load chains
10	$\{Cr_4\}$	3V Load Converter

Using the minimal cut sets as a guide, the RBD for Architecture #2 is displayed as **Figure 20**.

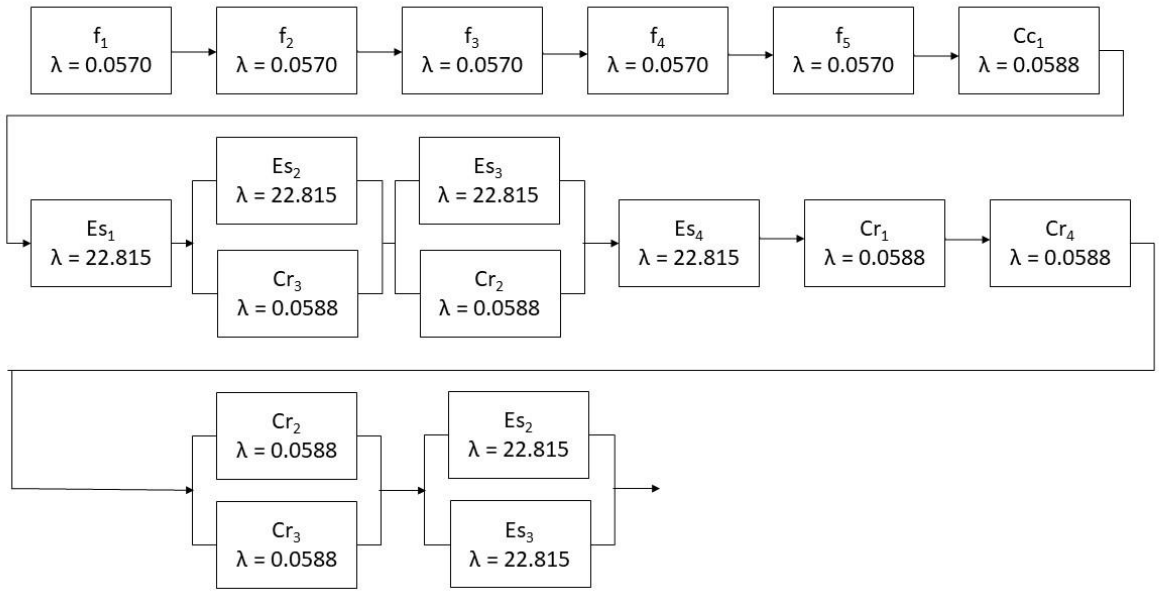

Figure 20—Architecture #2 RBD

The mathematics now for resolving the RBD for Architecture #2 become slightly more complex than the previous two architectures. The blocks that have two elements with different failure rates can be reduced to a single element using the inverse of (2-13) while the blocks with two elements with the same failure rate can be reduced using the inverse of (2-17). After the parallel blocks have been reduced to a single element, once again the entire relationship can be determined using (2-10). The relationship for determining the failure rate for Architecture #2 becomes

$$\lambda_{Arch\#2} = \lambda_{f_1} + \lambda_{f_2} + \lambda_{f_3} + \lambda_{f_4} + \lambda_{f_5} + \lambda_{Cc_1} + \lambda_{Es_1}$$
$$+ \frac{1}{\left(\frac{1}{\lambda_{Es_2}} + \frac{1}{\lambda_{Cr_3}} - \frac{1}{\lambda_{Es_2} + \lambda_{Cr_3}}\right)} + \frac{1}{\left(\frac{1}{\lambda_{Es_3}} + \frac{1}{\lambda_{Cr_2}} - \frac{1}{\lambda_{Es_3} + \lambda_{Cr_2}}\right)} \quad \textbf{(3-5)}$$
$$+ \lambda_{Es_4} + \lambda_{Cr_1} + \lambda_{Cr_4} + \frac{1}{\frac{1}{\lambda_{Cr}}\left(1 + \frac{1}{2}\right)} + \frac{1}{\frac{1}{\lambda_{Es}}\left(1 + \frac{1}{2}\right)}$$
$$= 61.458 \ \frac{Failures}{10^6 \ Hours}$$

and using (2-12) to determine the MTTF yields

$$MTTF_{Arch\#2} = \frac{1}{\lambda_{Arch\#2}} = \frac{1}{61.458} = 0.0163 \ x \ 10^6 \ Hours \quad \textbf{(3-6)}$$

An MTTF of 0.0163 x 10^6 Hours equals 1.856 years, a slight improvement over Architecture #1.

4.4 Architecture #3

Architecture #3 was presented as **Figure 9**. Architecture #3 becomes a truly distributed architecture by breaking out all of the PV panels into separate load chains. However, this architecture does not eliminate single points of failure. Further, the 3.3V load converters outputs are not tied together in this EPS. Both the minimal cut sets and RBD for Architecture #3 are identical to Architecture #1 but with the introduction of additional DC-DC Converter building blocks which are single points of failure. The minimal cut sets for Architecture #3 are summarized in **Table 16** and the RBD is displayed as **Figure 21**.

Table 16—Minimal Cut Sets for Architecture #3

Minimal Cut Set #	Minimal Cut Sets	Cut Set Description
1	$\{f_1\}, \{f_2\}, \{f_3\}, \{f_4\}, \{f_5\}$	Fuel Source - PV Array
2	$\{Cc_1\}$	DC-DC Boost Converter
3	$\{Cc_2\}$	DC-DC Boost Converter
4	$\{Cc_3\}$	DC-DC Boost Converter
5	$\{Cc_4\}$	DC-DC Boost Converter
6	$\{Es_1\}$	Li-Ion Battery
7	$\{Es_2\}$	Li-Ion Battery
8	$\{Es_3\}$	Li-Ion Battery
9	$\{Es_4\}$	Li-Ion Battery
10	$\{Cr_1\}$	5V Load Converter
11	$\{Cr_2\}$	3.3V Load Converter #1
12	$\{Cr_3\}$	3.3V Load Converter #2
13	$\{Cr_4\}$	3V Load Converter

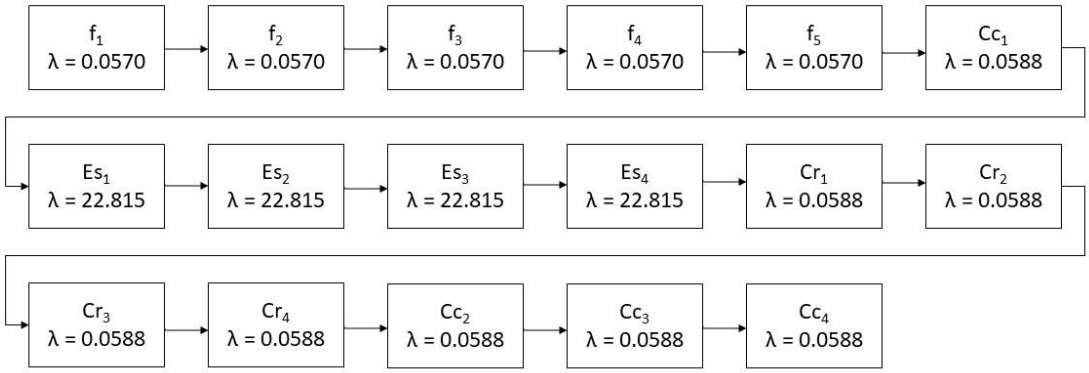

Figure 21—Architecture #3 RBD

Building on the equation for the failure rate from Architecture #1 (3-4) to calculate the overall system failure rate, both the failure rate and MTTF for Architecture #3 are calculated as

$$\lambda_{Arch\#3} = \lambda_{f_1} + \lambda_{f_2} + \lambda_{f_3} + \lambda_{f_4} + \lambda_{f_5} + \lambda_{Cc_1} + \lambda_{Es_1} + \lambda_{Es_2} + \lambda_{Es_3} + \lambda_{Es_4} + \lambda_{Cr_1} + \lambda_{Cr_2} + \lambda_{Cr_3} + \lambda_{Cr_4} + \lambda_{Cc_2} + \lambda_{Cc_3} + \lambda_{Cc_4} = 92.015 \frac{Failures}{10^6\ Hours} \quad \textbf{(3-7)}$$

$$MTTF_{Arch\#3} = \frac{1}{\lambda_{Arch\#3}} = \frac{1}{92.015} = 0.01087\ x\ 10^6\ Hours \quad \textbf{(3-8)}$$

An MTTF of 0.01087 x 10^6 Hours equals 1.239 years. Both Architecture #1 and #3 hold similar reliability metrics, but offer advantages in other ways, which will be discussed in more details in *Chapter 5.0*. Further, Architecture #3 is an important step in developing the other architectures under consideration.

4.5 Architecture #4

Architecture #4 was presented as **Figure 10**. This architecture ties the DC Links of the 3.3V output converters together in a redundant fashion. Architecture #4 is similar to Architecture #3 such that it also has a distributed topology. While Architectures #3 and #4 are similar in their distributed topologies, the latter adds the redundancy element of the outputs of the 3.3V load converters. With this setup, Architecture #4 builds on the reliability of Architecture #2 by making the fuel source, the PV panels, independent of one another. With this understanding, the minimal cut sets for Architecture #4 are displayed as **Table 17** and the RBD is shown as **Figure 22**.

Table 17—Minimal Cut Sets for Architecture #4

Minimal Cut Set #	Minimal Cut Sets	Cut Set Description
1	$\{f_1\}, \{f_2\}, \{f_5\}$	Single point of failure PV Panels
2	$\{Cc_1\}, \{Cc_4\}$	Single point of failure DC-DC converters
3	$\{Es_1\}, \{Es_4\}$	Single point of failure batteries
4	$\{Cr_1\}, \{Cr_4\}$	Single point of failure load converters
5	$\{f_3, f_4\}, \{f_3, Cc_3\}, \{f_3, Es_3\}, \{f_3, Cr_3\}$	Combination of fuel cell from load chain 2 and any component in load chain 3
6	$\{f_4, f_3\}, \{f_4, Cc_2\}, \{f_4, Es_2\}, \{f_4, Cr_2\}$	Combination of fuel cell from load chain 3 and any component in load chain 2
7	$\{Cc_2, Cc_3\}, \{Cc_2, Es_3\}, \{Cc_2, Cr_3\}$	Combination of DC-DC boost converter from load chain 2 and any component in load chain 3
8	$\{Cc_3, Es_2\}, \{Cc_3, Cr_2\}$	Combination of DC-DC boost converter from load chain 3 and any component in load chain 2
9	$\{Es_2, Es_3\}, \{Es_2\ Cr_3\}$	Combination of energy storage device in load chain 2 with any device in load chain 3
10	$\{Es_3, Cr_2\}$	Combination of energy storage device in load chain 3 with any device in load chain 2
11	$\{Cr_2, Cr_3\}$	Combination of DC-DC converter in load chain 2 with any device in load chain 3

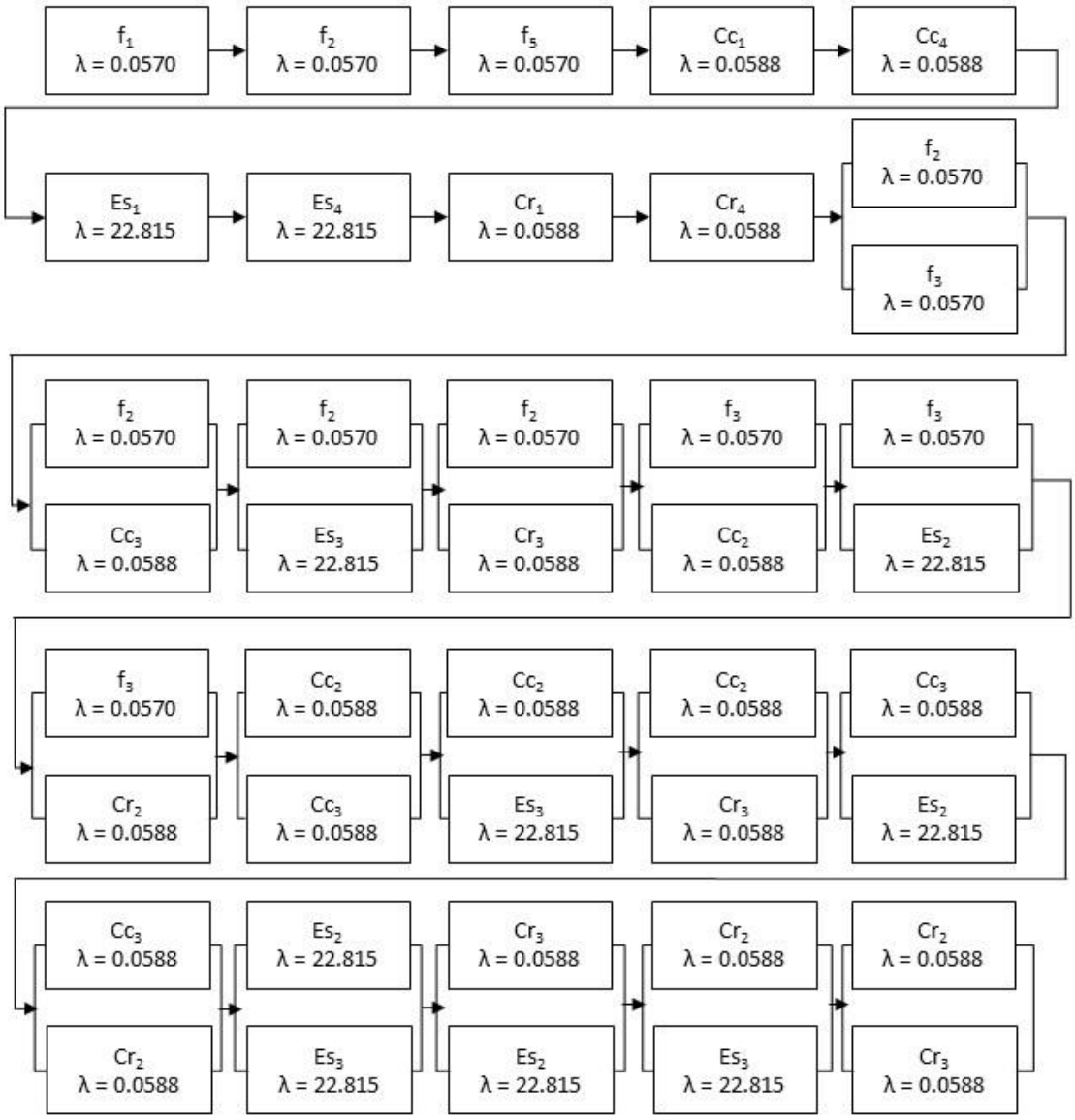

Figure 22—Architecture #4 RBD

For the sake of simplicity in writing out the reliability equation for the failure rate for Architecture #4, the "//" symbol will be used to represent elements in parallel. These elements will be reduced to a single series element through the inverse of (2-13) for elements with different failure rates and the inverse of (2-17) for elements that have the same failure rates. The relationship for the failure rate for Architecture #4 is then

$$\lambda_{Arch\#4} = \lambda_{f_1} + \lambda_{f_2} + \lambda_{f_5} + \lambda_{Cc_1} + \lambda_{Cc_4} + \lambda_{Es_1} + \lambda_{Es_4} + \lambda_{Cr_1} + \lambda_{Cr_4} + \lambda_{f_3}//\lambda_{f_4}$$
$$+ \lambda_{f_3}//\lambda_{Cc_3} + \lambda_{f_3}//\lambda_{Es_3} + \lambda_{f_3}//\lambda_{Cr_3} + \lambda_{f_4}//\lambda_{Cc_2} + \lambda_{f_4}//\lambda_{Es_2}$$
$$+ \lambda_{f_4}//\lambda_{Cr_2} + \lambda_{Cc_2}//\lambda_{Cc_3} + \lambda_{Cc_2}//\lambda_{Es_3} + \lambda_{Cc_2}//\lambda_{Cr_3} \quad \textbf{(3-9)}$$
$$+ \lambda_{Cc_3}//\lambda_{Es_2} + \lambda_{Cc_3}//\lambda_{Cr_2} + \lambda_{Es_2}//\lambda_{Es_3} + \lambda_{Cr_3}//\lambda_{Es_2}$$
$$+ \lambda_{Cr_2}//\lambda_{Es_3} + \lambda_{Cr_2}//\lambda_{Cr_3} = 61.945 \ \frac{Failures}{10^6 \ Hours}$$

$$MTTF_{Arch\#4} = \frac{1}{\lambda_{Arch\#4}} = \frac{1}{61.945} = 0.0161 \ x \ 10^6 \ Hours \quad \textbf{(3-10)}$$

An MTTF of 0.0161 x 10^6 Hours equals 1.842 years. Both Architecture #2 and #4 have similar reliability metrics, but hold advantages in other ways, which will be discussed in further detail in *Chapter 5.0*.

4.6 Architecture #5

Architecture #5 was presented as **Figure 11**. Architecture #5 is the same as Architecture #4 but now introduces the low voltage common bus at the outputs of the PV panels. With this topology, all but one PV panel (*koon*, in this case 1oo5) must be operational for the power system to function as intended. It is assumed for the sake of this analysis that one PV panel can support the functionality of the EPS. While this may not be wholly practical once launched in space, it is important to consider the reliability such an architecture may be able to provide from a system standpoint if the technology were properly developed and vetted.

The RBD for this architecture can be developed by leveraging the work done for Architecture #4. However, the interaction with the PV panels clearly must change. There are many combinations of a component in the 3.3V load chains failing as well as all of the PV panels but one failing, but these combinations do not always constitute the *minimal* cut set and therefore are not included in both the table of minimal cut sets or the RBD. With this in mind, both the table of minimal cut sets and RBD for Architecture #5 becomes less complex than Architecture #4. The minimal cut sets are summarized in **Table 18** and the RBD is displayed as **Figure 23**.

Table 18—Minimal Cut Sets for Architecture #5

Minimal Cut Set #	Minimal Cut Sets	Cut Set Description
1	$\{f_1, f_2, f_3, f_4, f_5\}$	All fuel sources must fail to lose power (1oo5 must be functional to maintain operation).
2	$\{Cc_1\}, \{Cc_4\}$	Single point of failure DC-DC converters
3	$\{Es_1\}, \{Es_4\}$	Single point of failure batteries
4	$\{Cr_1\}, \{Cr_4\}$	Single point of failure load converters
5	$\{Cc_2, Cc_3\}, \{Cc_2, Es_3\}, \{Cc_2, Cr_3\}$	Combination of DC-DC boost converter from load chain 2 and any component in load chain 3
6	$\{Cc_3, Es_2\}, \{Cc_3, Cr_2\}$	Combination of DC-DC boost converter from load chain 3 and any component in load chain 2
7	$\{Es_2, Es_3\}, \{Es_2\ Cr_3\}$	Combination of energy storage device in load chain 2 with any device in load chain 3
8	$\{Es_3, Cr_2\}$	Combination of energy storage device in load chain 3 with any device in load chain 2
9	$\{Cr_2, Cr_3\}$	Combination of DC-DC converter in load chain 2 with any device in load chain 3

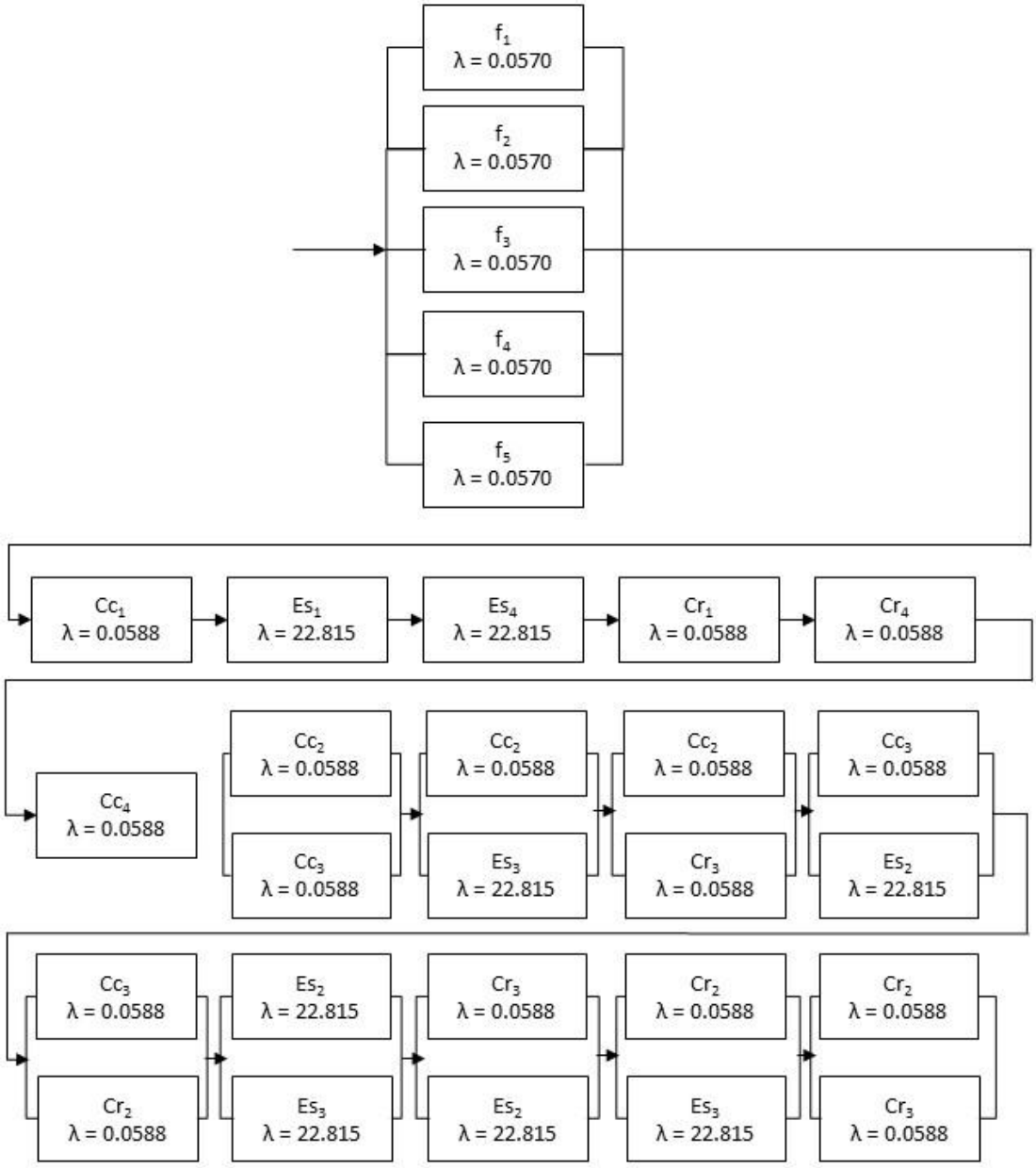

Figure 23—Architecture #5 RBD

Using the RBD to determine the relationship for the failure rate and (2-17) for a *koon* structure with 1oo5 (k =1 and n = 5) yields

$$\lambda_{Arch\#5} = \frac{1}{\frac{1}{\lambda_f}\left(1+\frac{1}{2}+\frac{1}{3}+\frac{1}{4}+\frac{1}{5}\right)} + \lambda_{Cc_1} + \lambda_{Cc_4} + \lambda_{Es_1} + \lambda_{Es_4} + \lambda_{Cr_1} + \lambda_{Cr_4}$$
$$+ \lambda_{Cc_2}//\lambda_{Cc_3} + \lambda_{Cc_2}//\lambda_{Es_3} + \lambda_{Cc_2}//\lambda_{Cr_3} + \lambda_{Cc_3}//\lambda_{Es_2} \quad \textbf{(3-11)}$$
$$+ \lambda_{Cc_3}//\lambda_{Cr_2} + \lambda_{Es_2}//\lambda_{Es_3} + \lambda_{Cr_3}//\lambda_{Es_2} + \lambda_{Cr_2}//\lambda_{Es_3}$$
$$+ \lambda_{Cr_2}//\lambda_{Cr_3} = 61.492\ \frac{Failures}{10^6\ Hours}$$

$$MTTF_{Arch\#5} = \frac{1}{\lambda_{Arch\#5}} = \frac{1}{61.492} = 0.0163\ x\ 10^6\ Hours \quad \textbf{(3-12)}$$

An MTTF of 0.0163 x 10^6 Hours equals 1.855 years, which is a slight improvement over Architecture #4, which was expected due to adding the redundancy of the PV panels in a parallel arrangement.

4.7 Architecture #6

Architecture #6 was presented as **Figure 12**. In this EPS, the low voltage bus on the PV panel array is applied only to the 3.3V load chains, referred to as load chain 2 and load chain 3. This is a distributed architecture again with the outputs of the 3.3V load converters tied together in parallel. While Architectures #5 and #6 are similar, it is important to make a distinction between the two. Since the increase in the MTTF with Architecture #5 can be considered marginal from previous distributed architectures established, it's important to determine a relative benefit of Architecture #5 to #6. From a technical feasibility standpoint, it is less complex to implement Architecture #6 than #5. The minimal cut sets for Architecture #6 are summarized in **Table 19** and the RBD is displayed as **Figure 24**.

Table 19—Minimal Cut Sets for Architecture #6

Minimal Cut Set #	Minimal Cut Sets	Cut Set Description
1	$\{f_1\}$, $\{f_2\}$, $\{f_5\}$	Single point of failure PV Panels
2	$\{Cc_1\}$, $\{Cc_4\}$	Single point of failure DC-DC converters
3	$\{Es_1\}$, $\{Es_4\}$	Single point of failure batteries
4	$\{Cr_1\}$, $\{Cr_4\}$	Single point of failure load converters
5	$\{f_3, f_4\}$	PV panels feeding load chains 2 and 3
6	$\{Cc_2, Cc_3\}$, $\{Cc_2, Es_3\}$, $\{Cc_2, Cr_3\}$, $\{Cc_3, Es_2\}$, $\{Cc_3, Cr_2\}$, $\{Es_2, Es_3\}$, $\{Es_2, Cr_3\}$, $\{Es_3, Cr_2\}$, $\{Cr_2, Cr_3\}$	Varying combinations of components in load chain 2 and load chain 3

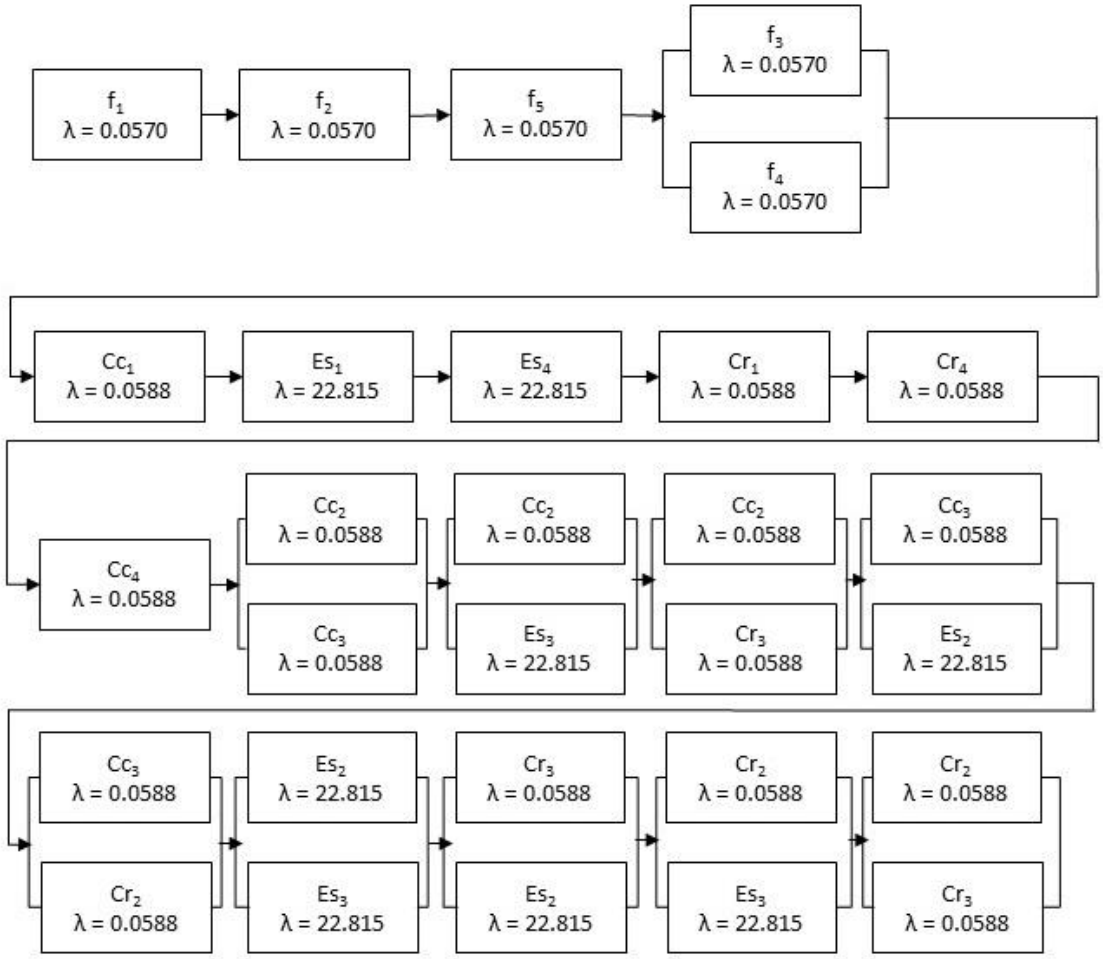

Figure 24—Architecture #6 RBD

Using (2-13) and (2-17) to reduce the parallel elements in the structure function to determine the failure rate yields

$$\lambda_{Arch\#6} = \lambda_{f_1} + \lambda_{f_2} + \lambda_{f_5} + \lambda_{Cc_1} + \lambda_{Cc_4} + \lambda_{Es_1} + \lambda_{Es_4} + \lambda_{Cr_1} + \lambda_{Cr_4} + \lambda_{f_3}//\lambda_{f_4} + \lambda_{Cc_2}//\lambda_{Cc_3} + \lambda_{Cc_2}//\lambda_{Es_3} + \lambda_{Cc_2}//\lambda_{Cr_3} + \lambda_{Cc_3}//\lambda_{Es_2} + \lambda_{Cc_3}//\lambda_{Cr_2} + \lambda_{Es_2}//\lambda_{Es_3} + \lambda_{Cr_3}//\lambda_{Es_2} + \lambda_{Cr_2}//\lambda_{Es_3} + \lambda_{Cr_2}//\lambda_{Cr_3} = 61.676 \frac{Failures}{10^6\ Hours} \quad \textbf{(3-13)}$$

$$MTTF_{Arch\#6} = \frac{1}{\lambda_{Arch\#6}} = \frac{1}{61.676} = 0.0162\ x\ 10^6\ Hours \quad \textbf{(3-14)}$$

An MTTF of 0.0162 x 10^6 Hours equals 1.8496 years, which is a very slight decrease in reliability from Architecture #5. Contrasting and comparison of these architectures will be outlined more in *Chapter 5.0*.

4.8 Architecture #7

Architecture #7 was presented as **Figure 13**. This architecture is nearly identical to Architecture #5, but introduces a crucial element of redundancy by putting the 3.3V load chain battery outputs in parallel with one another. As for a distributed architecture, this topology should provide the largest increase in MTTF thus far by creating redundancy of one of the most unreliable building blocks in the CubeSat EPS. It is assumed that the batteries in the 3.3V load chain cannot discharge into one another. The minimal cut sets for Architecture #7 are summarized in **Table 20** while the RBD is displayed as **Figure 25**.

Table 20—Minimal Cut Sets for Architecture #7

Minimal Cut Set #	Minimal Cut Sets	Cut Set Description
1	$\{f_1\}$, $\{f_2\}$, $\{f_5\}$	Single point of failure PV Panels
2	$\{Cc_1\}$, $\{Cc_4\}$	Single point of failure DC-DC converters
3	$\{Es_1\}$, $\{Es_4\}$	Single point of failure batteries
4	$\{Cr_1\}$, $\{Cr_4\}$	Single point of failure load converters
5	$\{f_3, f_4\}$	PV panels feeding load chains 2 and 3
6	$\{Cc_2, Cc_3\}$, $\{Es_2, Es_3\}$, $\{Cc_2, Cr_2, Cr_3\}$, $\{Cc_3, Cr_2, Cr_3\}$, $\{Cr_2, Cr_3\}$	Varying combinations of components in load chain 2 and load chain 3

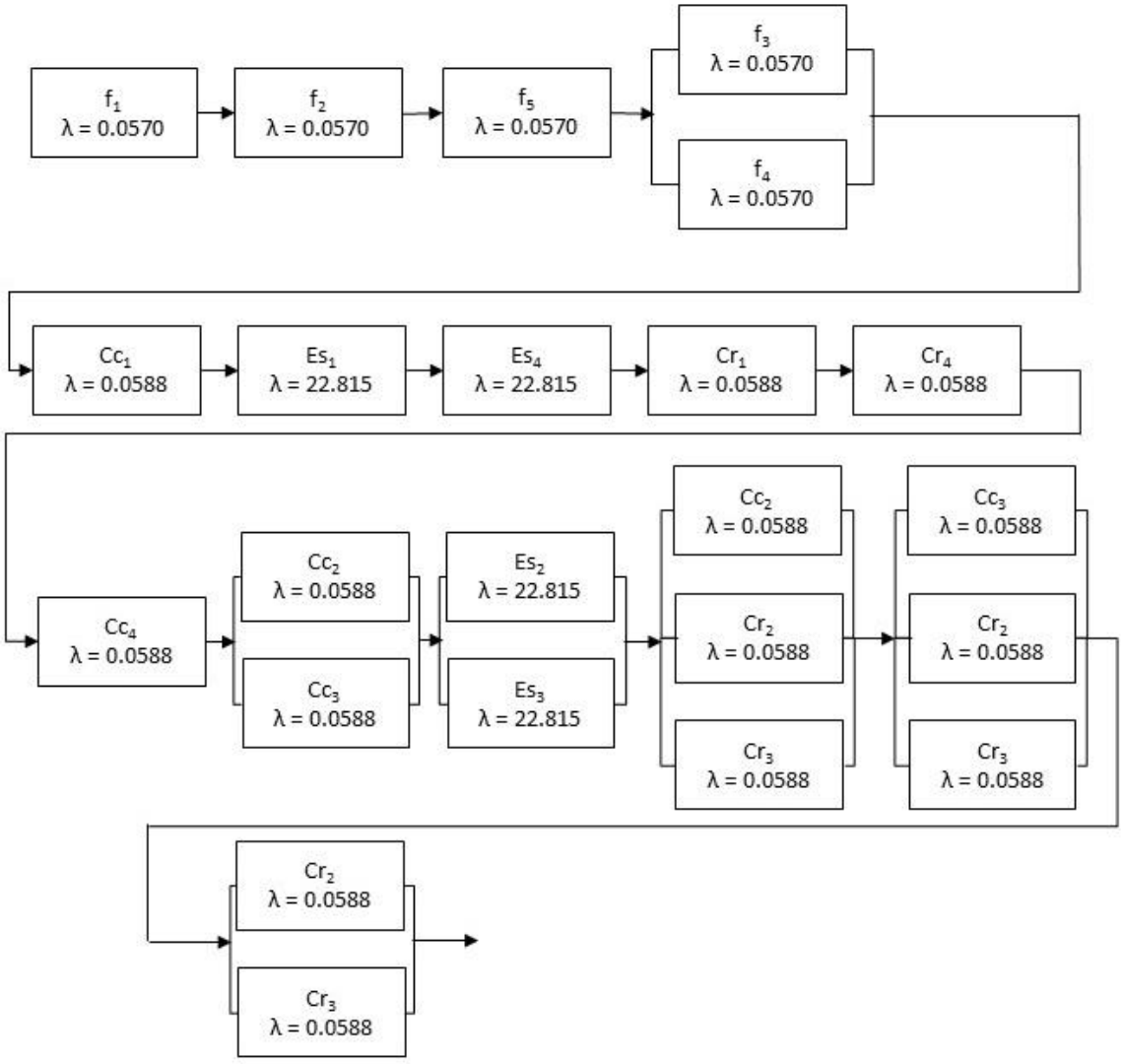

Figure 25—Architecture #7 RBD

Using the RBD to determine the relationship for the failure rate and (2-17) for a *koon* structure with 1oo3 (k =1 and n = 3) and 1oo2 (k=1 and n=2) yields

$$\lambda_{Arch\#7} = \lambda_{f_1} + \lambda_{f_2} + \lambda_{f_5} + \lambda_{Cc_1} + \lambda_{Cc_4} + \lambda_{Es_1} + \lambda_{Es_4} + \lambda_{Cr_1} + \lambda_{Cr_4} + \lambda_{f_3}//\lambda_{f_4}$$
$$+ \lambda_{Cc_2}//\lambda_{Cc_3} + \lambda_{Es_2}//\lambda_{Es_3} + \frac{1}{\frac{1}{\lambda_C}\left(1+\frac{1}{2}+\frac{1}{3}\right)} + \frac{1}{\frac{1}{\lambda_C}\left(1+\frac{1}{2}+\frac{1}{3}\right)} \quad \textbf{(3-15)}$$
$$+ \lambda_{Cr_2}//\lambda_{Cr_3} = 61.427\frac{Failures}{10^6\ Hours}$$

$$MTTF_{Arch\#7} = \frac{1}{\lambda_{Arch\#7}} = \frac{1}{61.427} = 0.0163\ x\ 10^6\ Hours \quad \textbf{(3-16)}$$

where λ_C is the failure rate for the DC-DC converter and an MTTF of 61.427 x 10^6 Hours equals 1.8571 years, which is only a very marginal improvement over Architecture #6.

4.9 Architecture #8

Architecture #8 was presented as **Figure 14**. This architecture further expands on Architecture #7 by introducing a low voltage bus tying all the battery building blocks together. It is expected that this topology should provide the best MTTF reliability metric up to this point, as this architecture adds a considerable amount of redundancy for the least reliable component and eliminates it as a single point of failure. Up to this point, only the 3.3V load chains could leverage battery redundancy by sharing this component. However, with this architecture, all load chains are sharing a total of 4 batteries. Again, it is assumed that no batteries can discharge into any other battery on the bus. It is further assumed that single element components, such as a single PV panel, is capable of handling the entire CubeSat EPS load if necessary. While unlikely, scenarios such as this could occur in this architecture and are outlined in the minimal cut sets, which are

summarized in **Table 21**. The RBD for this architecture is displayed across **Figure 26** and **Figure 27**.

Table 21—Minimal Cut Sets for Architecture #8

Minimal Cut Set #	Minimal Cut Sets	Cut Set Description
1	$\{f_1, f_2, f_3, f_4, f_5\}$	All PV panels must fail to lose energy harvesting. If only one fails, there is still energy flow to the battery bus.
2	$\{f_3, f_4, f_5, Cc_1\}$, $\{f_1, f_2, f_3, f_4, Cc_4\}$, $\{f_1, f_2, f_3, f_5, Cc_3\}$, $\{f_1, f_2, f_4, f_5, Cc_2\}$	Combination of fuel source and single point DC-DC boost converter
3	$\{f_3, f_4, f_5, Es_1\}$, $\{f_1, f_2, f_3, f_4, Es_4\}$, $\{f_1, f_2, f_4, f_5, Es_2\}$, $\{f_1, f_2, f_3, f_5, Es_3\}$	Combination of fuel cell source and single point Li-Ion battery failure
4	$\{Cc_2, Cc_3, Cc_4, Es_1\}$, $\{Cc_1, Cc_2, Cc_3, Es_4\}$, $\{Cc_1, Cc_2, Cc_4, Es_3\}$, $\{Cc_1, Cc_3, Cc_4, Es_2\}$	Combination of DC-DC boost converter and Li-Ion battery
5	$\{Cr_1\}$, $\{Cr_2, Cr_3\}$, $\{Cr_4\}$	If any output stage fails, mission fails
6	$\{Es_1, Es_2, Es_3, Es_4\}$	All batteries would need to fail for mission failure
7	$\{Cc_1, Cc_2, Cc_3, Cc_4\}$	All DC-DC boost converters would need to fail for mission failure.

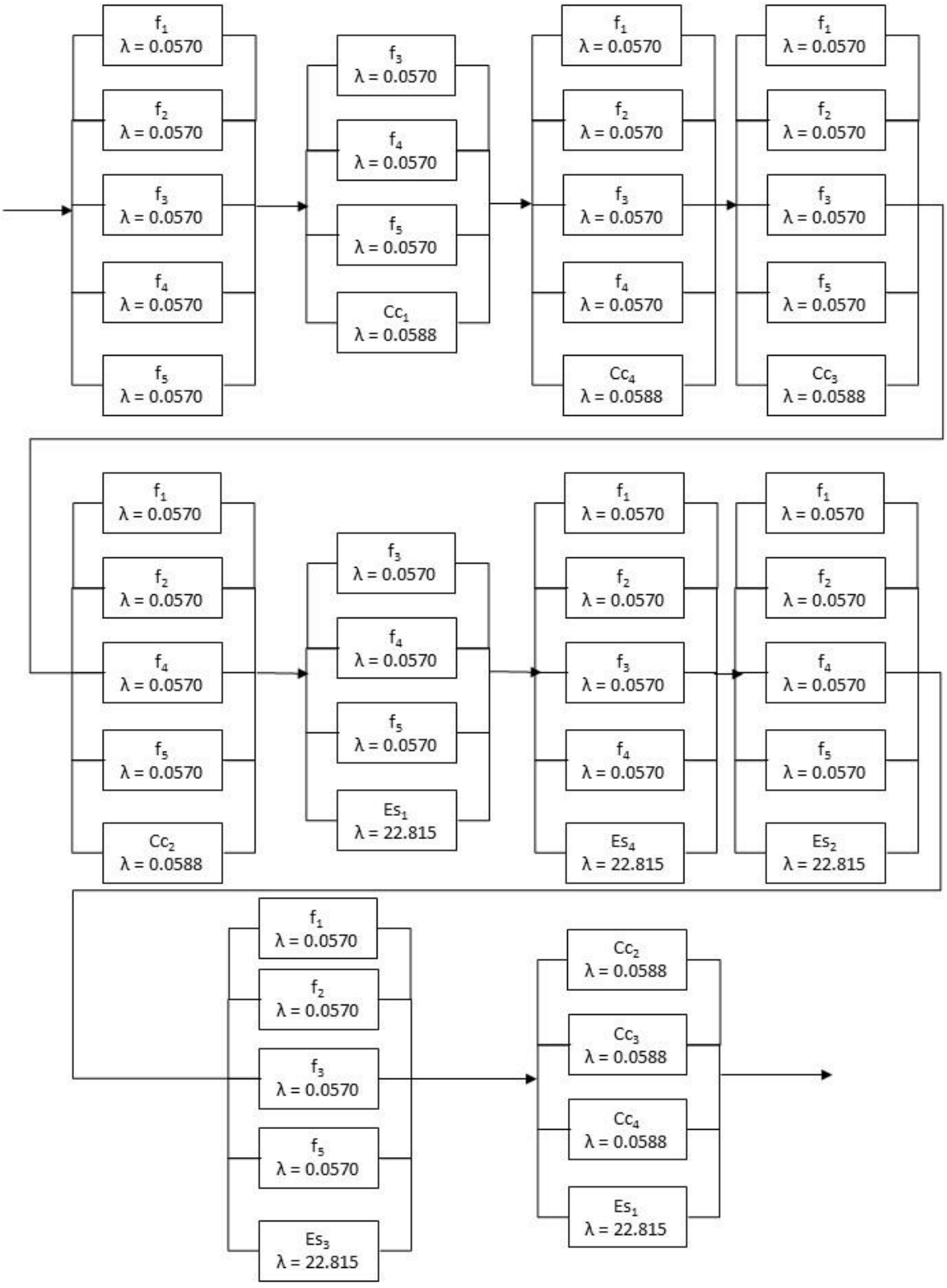

Figure 26—Architecture #8 RBD, part 1

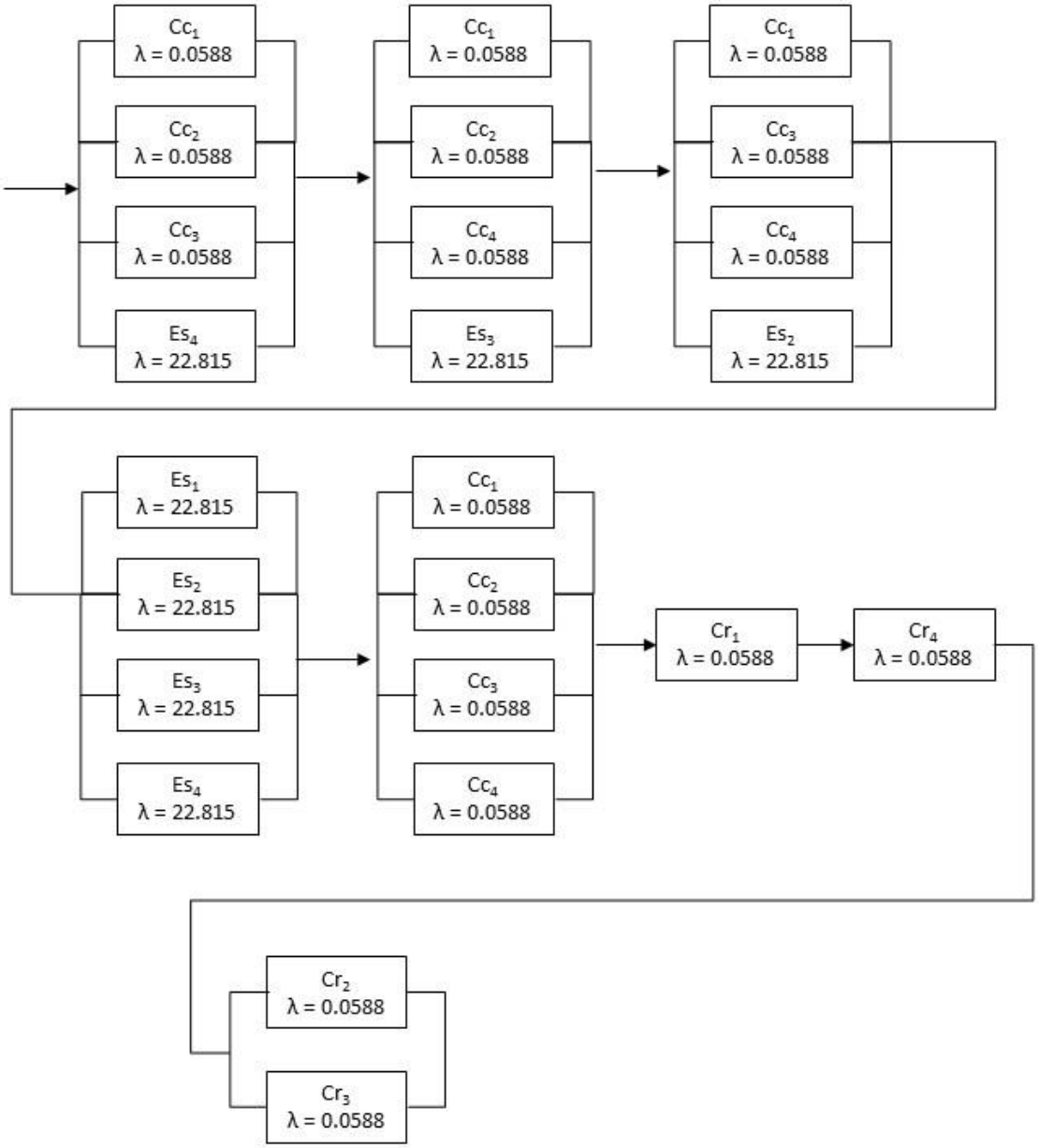

Figure 27—Architecture #8 RBD, part 2

To determine the relationship for the failure rate for Architecture #8, a combination of (2-13) and (2-17) will be used to reduce parallel element groupings to a single element. Since the majority of the parallel element combinations in the RBD are not all of the same failure rate, (2-

13) must be leveraged once the grouping is reduced to only two elements. To reduce to two elements, (2-17) is used for all elements with the same failure rate.

$$\lambda_{Arch\#8} = \frac{1}{\frac{1}{\lambda_f}\left(1+\frac{1}{2}+\frac{1}{3}+\frac{1}{4}+\frac{1}{5}\right)} + \frac{1}{\left(\frac{1}{\lambda_f}\left(1+\frac{1}{2}+\frac{1}{3}\right)\right)} // \lambda_{Cc_1}$$
$$+ \frac{1}{\left(\frac{1}{\lambda_f}\left(1+\frac{1}{2}+\frac{1}{3}+\frac{1}{4}\right)\right)} // \lambda_{Cc_4} + \frac{1}{\left(\frac{1}{\lambda_f}\left(1+\frac{1}{2}+\frac{1}{3}+\frac{1}{4}\right)\right)} // \lambda_{Cc_3}$$
$$+ \frac{1}{\left(\frac{1}{\lambda_f}\left(1+\frac{1}{2}+\frac{1}{3}+\frac{1}{4}\right)\right)} // \lambda_{Cc_2} + \frac{1}{\left(\frac{1}{\lambda_f}\left(1+\frac{1}{2}+\frac{1}{3}\right)\right)} // \lambda_{Es_1}$$
$$+ \frac{1}{\left(\frac{1}{\lambda_f}\left(1+\frac{1}{2}+\frac{1}{3}+\frac{1}{4}\right)\right)} // \lambda_{Es_4} + \frac{1}{\left(\frac{1}{\lambda_f}\left(1+\frac{1}{2}+\frac{1}{3}+\frac{1}{4}\right)\right)} // \lambda_{Es_2}$$
$$+ \frac{1}{\left(\frac{1}{\lambda_f}\left(1+\frac{1}{2}+\frac{1}{3}+\frac{1}{4}\right)\right)} // \lambda_{Es_3} + \frac{1}{\left(\frac{1}{\lambda_C}\left(1+\frac{1}{2}+\frac{1}{3}\right)\right)} // \lambda_{Es_1} \quad \textbf{(3-17)}$$
$$+ \frac{1}{\left(\frac{1}{\lambda_C}\left(1+\frac{1}{2}+\frac{1}{3}\right)\right)} // \lambda_{Es_4} + \frac{1}{\left(\frac{1}{\lambda_C}\left(1+\frac{1}{2}+\frac{1}{3}\right)\right)} // \lambda_{Es_3}$$
$$+ \frac{1}{\left(\frac{1}{\lambda_C}\left(1+\frac{1}{2}+\frac{1}{3}\right)\right)} // \lambda_{Es_2} + \frac{1}{\left(\frac{1}{\lambda_{Es}}\left(1+\frac{1}{2}+\frac{1}{3}+\frac{1}{4}\right)\right)}$$
$$+ \frac{1}{\left(\frac{1}{\lambda_C}\left(1+\frac{1}{2}+\frac{1}{3}+\frac{1}{4}\right)\right)} + \lambda_{Cr_1} + \lambda_{Cr_4} + \lambda_{Cr_1} // \lambda_{Cr_3}$$
$$= 11.50 \ \frac{Failures}{10^6 \ Hours}$$

$$MTTF_{Arch\#8} = \frac{1}{\lambda_{Arch\#8}} = \frac{1}{11.50} = 0.0870\ x\ 10^{6}\ Hours \quad \textbf{(3-18)}$$

An MTTF of 0.0870 x 10^6 Hours equals 9.92 years, a vast and expected increase in the MTTF for this EPS configuration.

4.10 Architecture #9

Architecture #8 was presented as **Figure 15**. This architecture builds on Architecture #8 by introducing a low voltage bus across all of the PV panels. The advantage in this architecture is now PV panel redundancy is introduced, and the entire PV array can be properly load balanced in the instance of individual panel failures. This architecture is not expected to have a significant reliability metric improvement above Architecture #8, however various technical implications may be a factor in selection of this architecture, which will be outlined in more detail in *Chapter 5.0* The minimal cut sets for Architecture #9 are summarized in **Table 22** and the RBD is displayed as **Figure 28**. By introducing the low voltage bus across the PV panels, both the minimal cut sets and RBD become much less complex than Architecture #8.

Table 22—Minimal Cut Sets for Architecture #9

Minimal Cut Set #	Minimal Cut Sets	Cut Set Description
1	$\{f_1, f_2, f_3, f_4, f_5\}$	All PV panels would need to fail to have a mission failure
2	$\{Cc_1, Cc_2, Cc_3, Cc_4\}$	All DC-DC boost converters would need to fail to have a mission failure
3	$\{Es_1, Es_2, Es_3, Es_4\}$	All batteries would need to fail to have a mission failure
4	$\{Cr_1\}, \{Cr_2, Cr_3\}, \{Cr_4\}$	Output converters still remain as single points of failures for load chain 1 and load chain 4.

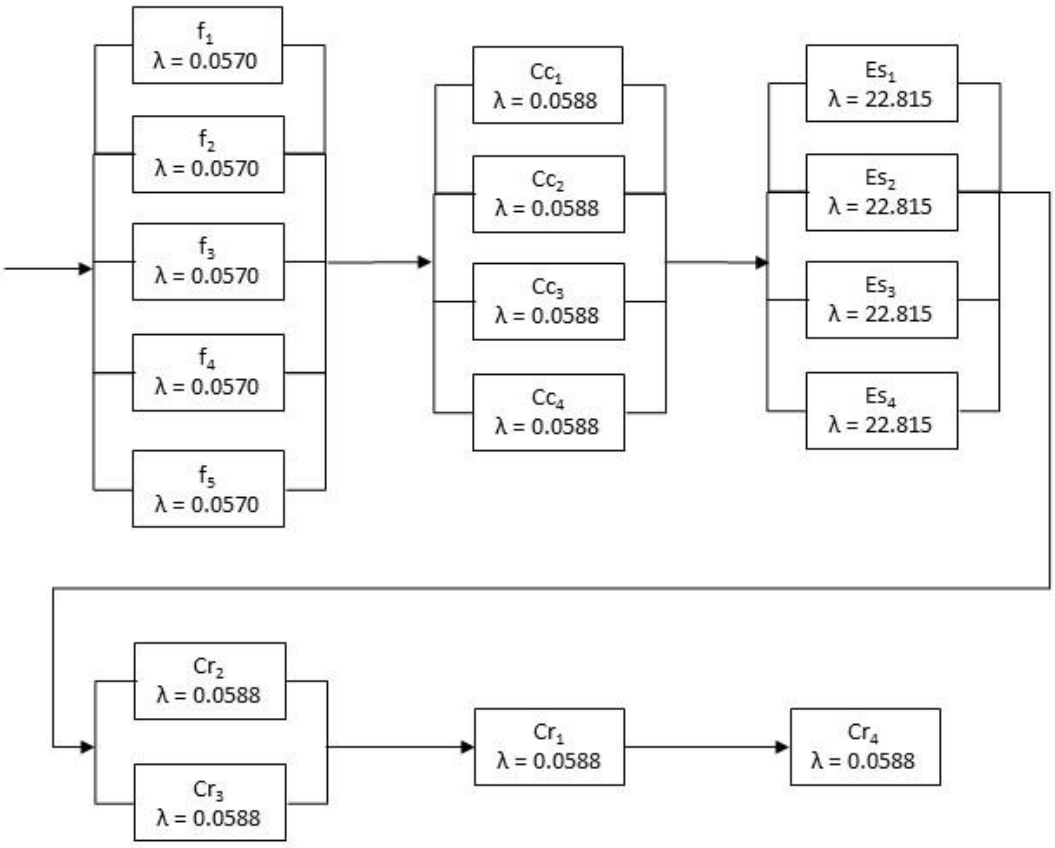

Figure 28—Architecture #9 RBD

Using the appropriate relationships, the failure rate for this architecture is determined to be

$$\lambda_{Arch\#9} = \frac{1}{\frac{1}{\lambda_f}\left(1+\frac{1}{2}+\frac{1}{3}+\frac{1}{4}+\frac{1}{5}\right)} + \frac{1}{\frac{1}{\lambda_c}\left(1+\frac{1}{2}+\frac{1}{3}+\frac{1}{4}\right)} + \frac{1}{\frac{1}{\lambda_{Es}}\left(1+\frac{1}{2}+\frac{1}{3}+\frac{1}{4}\right)} + \lambda_{Cr_2}//\lambda_{Cr_3} + \lambda_{Cr_1} + \lambda_{Cr_2} = 11.161\frac{Failures}{10^6\ Hours} \quad \textbf{(3-19)}$$

$$MTTF_{Arch\#9} = \frac{1}{\lambda_{Arch\#9}} = \frac{1}{11.161} = 0.0890\ x\ 10^6\ Hours \quad \textbf{(3-20)}$$

An MTTF of 0.0890 x 10^6 Hours equals 10.221 years, a continued improvement from previous EPS topologies.

4.11 Architecture #10

Architecture #10 was presented as **Figure 16**, which is the final architecture under consideration in this study. The configuration for this architecture introduces individual common buses for the PV panels, DC-DC boost converters, and Li-Ion batteries. There is also a common output bus for the 3.3V load converters, but the 5V and 3V outputs remain independent. At first glance, it might be expected that this architecture will provide the highest reliability metric in this thesis. However, the minimal cut sets and subsequently the RBD for Architecture #10 is exactly the same as Architecture #9. This is because both of these architectures can act in a similar way for power flow; that is, the common bus on the output of the Li-Ion batteries ultimately can route

power flow where needed in both cases. The main difference, however, is that Architecture #10 provides more capability to properly load balance whenever failures of independent components occur. This will be discussed in more detail in *Chapter 5.0*.

For posterity, the minimal cut sets for Architecture #10 are summarized in **Table 23** and the RBD is displayed in **Figure 29**.

Table 23—Minimal Cut Sets for Architecture #10

Minimal Cut Set #	Minimal Cut Sets	Cut Set Description
1	$\{f_1, f_2, f_3, f_4, f_5\}$	All PV panels would need to fail to have a mission failure
2	$\{Cc_1, Cc_2, Cc_3, Cc_4\}$	All DC-DC boost converters would need to fail to have a mission failure
3	$\{Es_1, Es_2, Es_3, Es_4\}$	All batteries would need to fail to have a mission failure
4	$\{Cr_1\}, \{Cr_2, Cr_3\}, \{Cr_4\}$	Output converters still remain as single points of failures for load chain 1 and load chain 4.

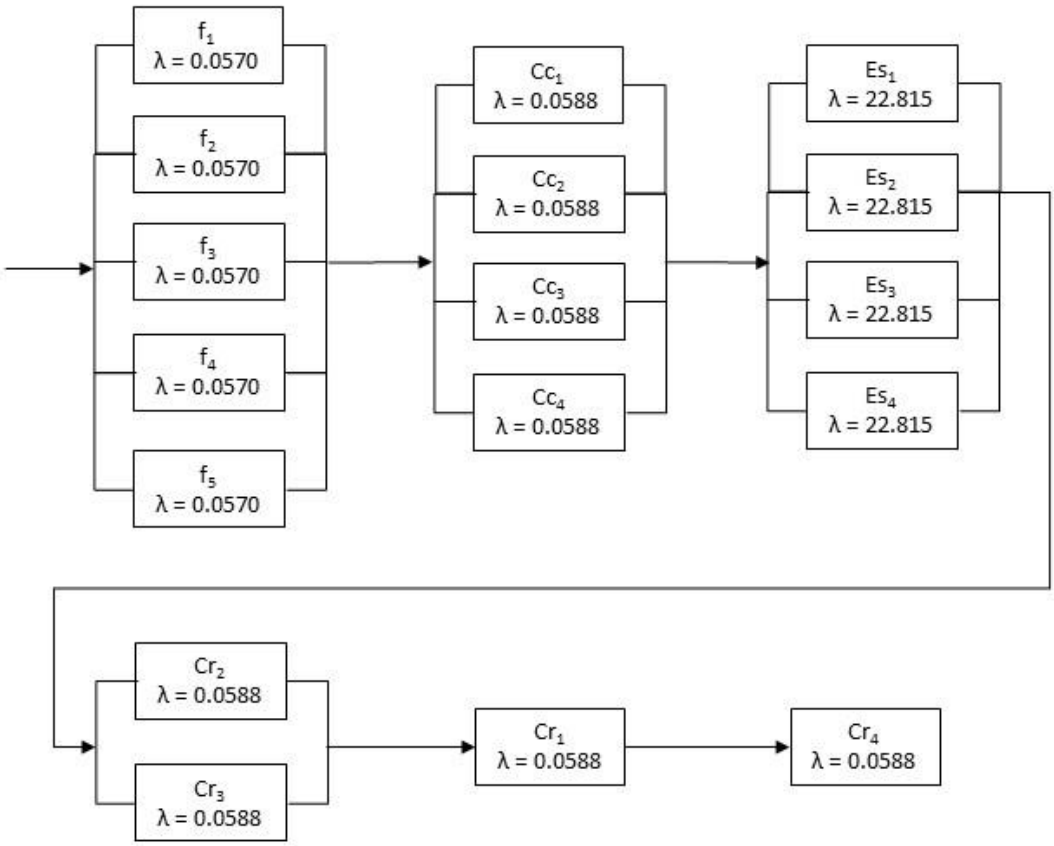

Figure 29—Architecture #10 RBD

Since Architecture #9 and #10 share the same RBD, the failure rate relationship for Architecture #10 is simply

$$\lambda_{Arch\#10} = \lambda_{Arch\#9} = 11.161 \frac{Failures}{10^6\ Hours} \quad \textbf{(3-21)}$$

$$MTTF_{Arch\#10} = \frac{1}{\lambda_{Arch\#10}} = \frac{1}{11.161} = 0.0890\ x\ 10^6\ Hours \quad \textbf{(3-22)}$$

As mentioned, creating the low voltage bus for the DC-DC boost converter outputs does not impact the reliability metric, and the MTTF for Architecture #10 is 0.0890 x 10^6 Hours, which is 10.221 years.

4.12 EPS Architectures Reliability Metrics Summary

With the reliability metrics calculated (Failure Rate, λ, and MTTF) for each ESP architecture, a strong comparison can finally be made across all alternatives from the baseline. A chart summarizing the architecture reliability metrics in order from longest to shortest MTTF is displayed as **Figure 30**. This chart will be referred to often in *Chapter 5.0*, where conclusions are drawn about the viability of each architecture. **Table 24** summarizes the reliability metrics numerically.

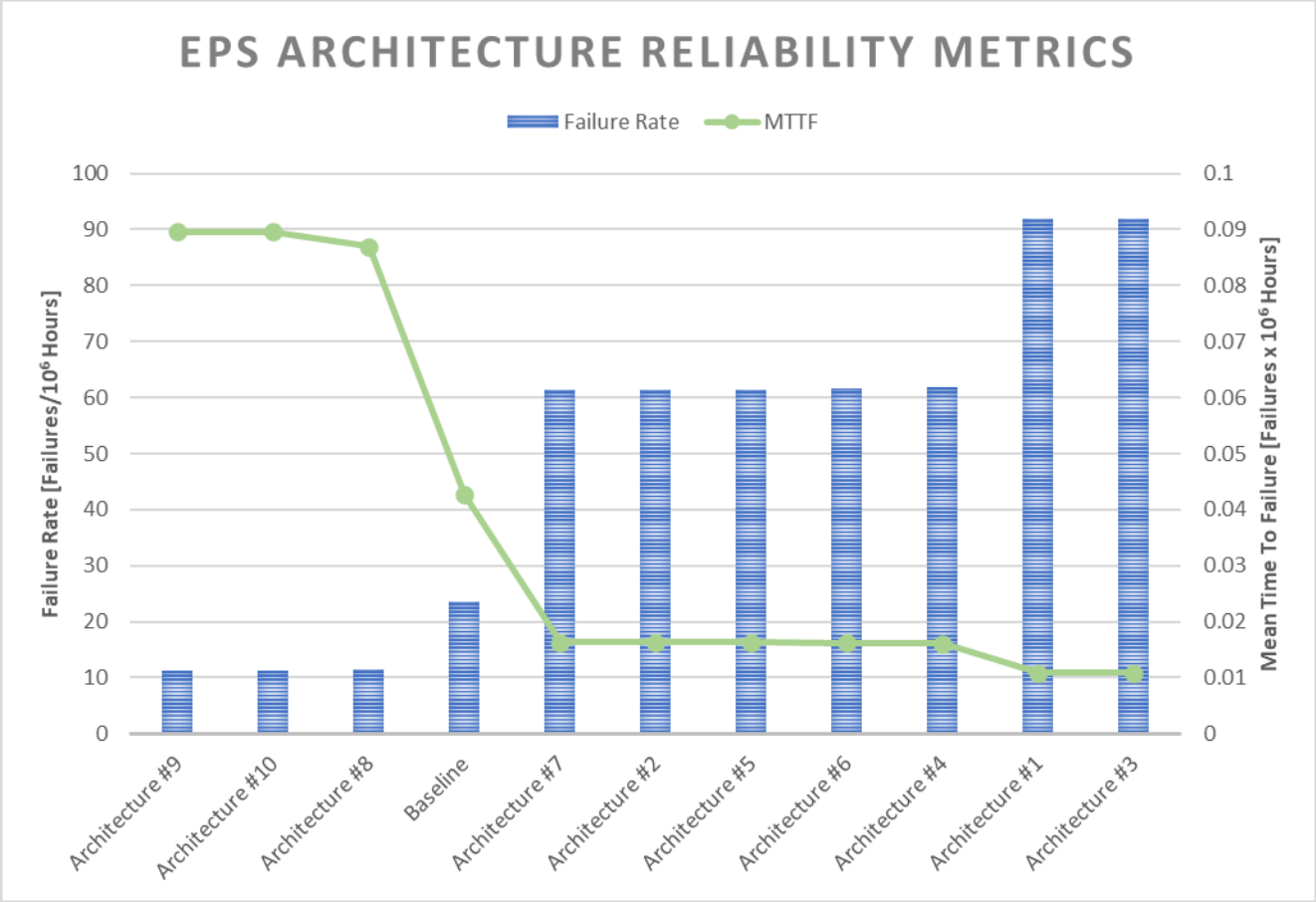

Figure 30—Summary of EPS Architecture Reliability Metrics

Table 24—Summary of Reliability Metrics For All Architectures

	Failure Rate	MTTF	Years
Architecture #9	11.161	0.08960	10.221
Architecture #10	11.161	0.08960	10.221
Architecture #8	11.500	0.08695	9.919
Baseline	23.453	0.04264	4.864
Architecture #7	61.427	0.01628	1.857
Architecture #2	61.458	0.01627	1.856
Architecture #5	61.492	0.01626	1.855
Architecture #6	61.676	0.01621	1.850
Architecture #4	61.945	0.01614	1.842
Architecture #1	91.839	0.01089	1.242
Architecture #3	92.015	0.01087	1.240

5.0 Conclusions and Comparisons

5.1 Best Reliability Metrics

As expected, the architectures including Li-Ion Battery Building Block redundancy ultimately had the most desirable reliability metrics. With Architectures #8, #9, and #10, the MTTF more than doubled from the baseline (4.864 years for the baseline versus 10.221 years for Architectures #9 and #10). By introducing a common Low Voltage battery bus that all Li-Ion batteries could contribute energy flow into, the overall reliability increased greatly.

Such a design change does not come easily, however. Not only does increasing the number of batteries by four times become much more cost prohibitive, but the technical complexity of the architecture vastly increases. When developing a complex architecture several issues regarding control, stability, power flow, hardware arrangement, and verification and validation occur. While simply adding building blocks on paper to introduce redundancy can make for successful reliability calculations, development of such a system can become a complex task.

However, as mentioned at the beginning of this thesis, the purpose was to study what improvements could be made from the traditional architecture baseline and be used as a starting point for an overall improved system.

5.2 Pros and Cons of Distributed Architectures

With this study, the majority of the alternate architectures introduced were of a distributed nature. That is, each load chain for the most part was broken out independently. This concept truly begins starting with Architecture #3 (shown in **Figure 3**) and is apparent in all subsequent architectures.

The benefit to a truly distributed architecture in this scenario is the ability to decouple loads from having a dependency on a single point of failure. While a CubeSat system may not have any systems deemed non-critical by a developer, it may still be able to operate if it loses certain payloads or functionalities. For example, a CubeSat could lose the functionality of an on-board camera system used for capturing high-resolution images in outer space, but it could not maintain proper functionality if it lost a control instrument such as gyroscope. If non-critical payload could be successfully decoupled from mission critical system components, the decreased calculated reliability may be worth the investment for keeping CubeSats functional longer. However, further study and development would be required—without the introduction and development of a common battery bus within the distributed architecture, a distributed architecture has a failure rate of nearly three times the baseline (23.453 Failures/10^6 Hours versus roughly 61 Failures/10^6 Hours for Architectures #7, #2, #5, #6, and #4) and nearly five times the baseline for architectures with no redundancy (23.453 Failures/10^6 Hours versus roughly 92 Failures/10^6 Hours for Architectures #1 and #3).

One simple (and free) change that can be made to benefit redundancy without added complexity is trying a common DC Link output for the 3.3V load chains. By simply sharing a common link between these two load chains, a large benefit in the reliability metric can be made. As shown in **Figure 30**, the distributed architectures with the DC Links of the 3.3V load chains

tied together have nearly two-thirds the failure rate of the two architectures that do not. Such a change comes nearly free but with a huge reliability benefit, and when applicable, should always be implemented if practical.

5.3 Rank of Architectures by Reliability Metrics and Final Conclusion

Several factors must be taken into account when determining the most viable architecture for future development or investigation. Overall Mean Time To Failure (MTTF), cost, system flexibility, and technical complexity are the chief factors under discussion here. To visualize the study results, **Table 25** presents a color-coded view of the architectures where green is favorable, yellow is neutral, and red is unfavorable. This chart offers a quick overview of the overall system factors of development.

Table 25—System Architecture Metrics (Color Coded for Favorability)

	MTTF	Cost	Flexibility	Complexity
Architecture #9				
Architecture #10				
Architecture #8				
Baseline				
Architecture #7				
Architecture #2				
Architecture #5				
Architecture #6				
Architecture #4				
Architecture #1				
Architecture #3				

Depending upon what system developer and engineering team decide is their most important factor of development (e.g., reliability such as MTTF), a decision can be made to

develop the most appropriate architecture for a specific application. Different applications may call for a different approach to be taken. As for the case mentioned in *Chapter 1.0* regarding CubeSat development for Mars, a system with a high cost but best MTTF is likely the appropriate choice. For a system used in LEO for more trivial exploration, such as capturing images of the Earth's surface, a system with a low and more favorable cost but poorer MTTF may be the best choice for this application.

Finally, concepts from this thesis can be used to develop other alternate architecture types. It was determined that additional building blocks such as the DC-DC converter don't greatly impact the reliability metric unless configured in a way to afford energy flow redundancy. Therefore, a developer may decide to add more redundancy where it has a larger impact, such as the Li-Ion battery, and focus effort of development in that area. It was shown that by introducing a Low Voltage battery bus where all batteries can contribute to power flow had a considerably large impact on the MTTF. Considering the technical challenges of achieving a successful version of such an architecture, a system architect and developer may be best suited to spend their time and energy focused in this area.

The vastness of space represents infinity. There are countless possibilities for development of systems to explore further frontiers. Simple changes made to improve a system reliability could ultimately lead to a discovery far in the reaches of space, such as Mars, that open doors for humankind that have never before been dreamed of.

Bibliography

[1] Toorian, K. Diaz and S. Lee, "The CubeSat Approach to Space Access," 2008 IEEE Aerospace Conference. Big Sky, MT, 2008, pp. 1-14, doi: 10.1109/AERO.2008.4526293.

[2] Kulu, E. *Nanosats Database*. April 4, 2021, Accessed on July 15, 2021 [Online]. Available: https://www.nanosats.eu/database

[3] E. Mabrouk, "What are SmallSats and CubeSats?," NASA, August 7, 2017. Accessed on: November 11, 2020. [Online]. Available: https://www.nasa.gov/content/what-are-smallsats-and-cubesats

[4] CDS, *CubeSat Design Specification, Rev. 13*. California Poly-Technic State University, 2015.

[5] J. Bester, B. Groenewald, R. Wilkinson, "Electrical power system for a 3U CubeSat nanosatellite incorporating peak power tracking with dual redundant control," Przeglad Elektrotechniczny (Electrical Review), 2021, ISSN 0033-2097, R. 88 NR 4a/2012

[6] J. Lee, E. Kim and K. G. Shin, "Design and Management of Satellite Power Systems," 2013 IEEE 34th Real-Time Systems Symposium, Vancouver, BC, 2013, pp. 97-106, doi: 10.1109/RTSS.2013.18.

[7] G. A. Landis, S. G. Bailey and R. Tischler, "Causes of Power-Related Satellite Failures," *2006 IEEE 4th World Conference on Photovoltaic Energy Conference*, Waikoloa, HI, 2006, pp. 1943-1945, doi: 10.1109/WCPEC.2006.279878.

[8] Langer, M., Bouwmeester, J. (2016). Reliability of CubeSats – Statistical Data, Developers' Beliefs and the Way Forward. Proceedings of the AIAA/USU Conference on Small Satellites, SSC16-X-2.

[9] Lashab, A., Sera D., and Guerrero, J. M., "A Dual-Discrete Model Predictive Control-Based MPPT for PV Systems," in *IEEE Transactions on Power Electronics*, vol. 34, no. 10, pp. 9686-9697, Oct. 2019, doi: 10.1109/TPEL.2019.2892809.

[10] Knap, V.; Vestergaard, L.K.; Stroe, D.-I. A Review of Battery Technology in CubeSats and Small Satellite Solutions. *Energies* **2020**, *13*, 4097. https://doi.org/10.3390/en13164097

[11] Lashab, A., Yaqoob, M., Terriche, Y., Vasquez, J. C., & Guerrero, J. M. (2020). Space Microgrids: New Concepts on Electric Power Systems for Satellites. IEEE Electrification Magazine.

[12] Komarek, T., Bailey, Z., Schone, H., Jedrey, T., Chandler, A. (2013). Novel Ideas for Exploring Mars with CubeSats: Challenges and Possibilities, presented at Low Cost Planetary Missions (LCPM), Pasadena, California, 2013. NASA.

[13] Rausand, Marvin. Reliability of Safety-Critical Systems: Theory and Applications, John Wiley & Sons, Incorporated, 2014. ProQuest Ebook Central, https://ebookcentral.proquest.com/lib/pitt-ebooks/detail.action?docID=1637653.

[14] Lundteigen, M.A. & Rausand, M. (2015). Reliability of Safety-Critical Systems – 5.1 Reliability Quantification with RBDs. Norwegian University of Science and Technology.

[15] United States of America Department of Defense (1991). *Military Handbook – Reliability Prediction of Electronic Equipment*. (MIL-HDBK-217F).

[16] S. Acharya et al., "Modeling and Design of Electrical Power Subsystem for CubeSats," 2019 International Conference on Smart Energy Systems and Technologies (SEST), 2019, pp. 1-6, doi: 10.1109/SEST.2019.8849042.

[17] Libal, A. *The Temperatures of Outer Space Around the Earth*. April 13, 2018, Accessed on August 21, 2021 [Online]. Available: https://sciencing.com/temperatures-outer-space-around-earth-20254.html

[18] Harris, Stephen J., Harris, David J., Li, Chen. "Failure Statistics for Commercial Litium Ion Batteries: A Study of 24 Pouch Cells." Journal of Power Sources. Volume 342. (2017): pages 589-597. https://doi.org/10.1016/j.jpowsour.2016.12.083.

[19] Knap, Vaclav & Vestergaard, Lars & Stroe, Daniel-Ioan. (2020). A Review of Battery Technology in CubeSats and Small Satellite Solutions. Energies. 13. 4097. 10.3390/en13164097.

[20] Jordan, Dirk C., Silverman, Timothy J., Wohlgemuth, John H., Kurtz, Sarah R., and VanSant, Kaitlyn T.. Photovoltaic failure and degradation modes. United States: N. p., 2017. Web. https://doi.org/10.1002/pip.2866.

[21] Rausand, M. and Høyland, A. *System Reliability Theory: Models, Statistical Methods, and Applications.* 2nd ed., John Wiley & Sons, 2004.

[22] M. Evzelman, M. M. Ur Rehman, K. Hathaway, R. Zane, D. Costinett and D. Maksimovic, "Active Balancing System for Electric Vehicles With Incorporated Low-Voltage Bus," in *IEEE Transactions on Power Electronics*, vol. 31, no. 11, pp. 7887-7895, Nov. 2016, doi: 10.1109/TPEL.2015.2513432.